PALEOCLIMATIC INVESTIGATION OF KARAIN CAVE (ANTALYA) USING STALAGMITE DATA

A THESIS SUBMITTED TO
THE GRADUATE SCHOOL OF NATURAL AND APPLIED SCIENCES
OF
MIDDLE EAST TECHNICAL UNIVERSITY

BY

EVREN TÜRKMENOĞLU

IN PARTIAL FULFILLMENT OF THE REQUIREMENTS
FOR
THE DEGREE OF MASTER OF SCIENCE
IN
ARCHAEOMETRY

JANUARY 2024

Approval of the thesis:

PALEOCLIMATIC INVESTIGATION OF KARAIN CAVE (ANTALYA) USING STALAGMITE DATA

submitted by **EVREN TÜRKMENOĞLU** in partial fulfillment of the requirements for the degree of **Master of Science** i**n Archeometry, Middle East Technical University** by,

Prof. Dr. Halil Kalıpçılar
Dean, **Graduate School of Natural and Applied Sciences** _____

Assoc. Prof. Dr. Ayşe Duman
Head of the Department, **Archeometry** _____

Prof. Dr. Gülay Ertaş
Supervisor, **Archeometry, METU** _____

Examining Committee Members:

Prof. Dr. Kaan Sayıt
Geological Engineering, METU _____

Prof. Dr. Gülay Ertaş
Chemistry, METU _____

Assoc. Prof. Dr. Zehra Semra Karakaş
Geological Engineering, Ankara University _____

Date: 26.01.2024

I hereby declare that all information in this document has been obtained and presented in accordance with academic rules and ethical conduct. I also declare that, as required by these rules and conduct, I have fully cited and referenced all material and results that are not original to this work.

Name Last name : Evren Türkmenoğlu

Signature :

ABSTRACT

PALEOCLIMATIC INVESTIGATION OF KARAIN CAVE (ANTALYA) USING STALAGMITE DATA

Türkmenoğlu, Evren
Master of Science, Archeometry
Supervisor : Prof. Dr. Gülay Ertaş

January 2024, 74 pages

This study investigates a stalagmite obtained from the Karain cave to understand its significance for paleoclimatologic reconstructions. Mineralogical, petrographical and chemical properties of the stalagmite are investigated using a petrographic microscope, scanning electron microscope (SEM-EDX), X-ray powder diffraction analysis (XRD), oxygen-, carbon- stable isotope analysis and Th/U radiometric age dating by using test samples collected along the growth axis of the stalagmite.

The results of the petrographic microscope, scanning electron microscope (SEM-EDX), and X-ray powder diffraction analysis (XRD) show that calcite is the major carbonate mineral that forms hard and compact layers along the growth axis of the stalagmite. It exhibits elongated and equant shapes and in some calcite layers fluid inclusions are present. Minor amounts of iron oxide, clay minerals and aragonite accompanied by porous texture form thin laminations alternating with calcite layers. These features correspond to hiatuses due to fluctuations in paleoclimatic and paleoenvironmental conditions.

Variations of the $\delta^{13}C$ and $\delta^{18}O$ ratios obtained along the stalagmite growth axis based on the Stable Isotope Analysis are almost co-variant and are characterized by minor fluctuations. The $\delta^{18}O$ and $\delta^{13}C$ values range between -3.27‰ to -4.74‰ and -2.13‰ to -5.44‰, respectively. More enriched $\delta^{18}O$ values indicate slightly cooler and dryer climate conditions that may be associated with C4 (grassland) type plants in the cave environment. However, when the $\delta^{18}O$ ratios become slightly depleted, they indicate more warm and wet climates associated with C3 (forest) type of plants. Except for these minor differences in the $\delta^{18}O$ ratios, measurements showed no significant climatic reversals recorded by the stalagmite sample.

Keywords: Stalagmite, Paleoclimate, Paleoenvironment, Karain Cave, Antalya

ÖZ

KARAİN MAĞRASI'NIN (ANTALYA) DİKİT VERİLERİ KULLANILARAK PALEOİKLİMSEL İNCELENMESİ

Türkmenoğlu, Evren
Yüksek Lisans, Arkeometri
Tez Yöneticisi: Prof. Dr. Gülay Ertaş

Ocak 2024, 74 sayfa

Bu çalışmada Karain mağarasına ait bir dikit örneğinin paleoiklim ve paleoçevresel özelliklerin anlaşılmasındaki önemi araştırılmıştır. Dikitin büyüme ekseni doğrultusunda alınan örneklerin mineralojik, petrografik ve kimyasal özellikleri petrografik mikroskop, tarama elektron mikroskop (SEM-EDX), X-ışınları toz difraktometresi (XRD), oksijen-karbon duyarlı izotop analizleri, ve Th/U radyometrik yaş tayini yapılmıştır.

Petrografik mikroskop, tarama elektron mikroskop (SEM-EDX) ve X-ışınları toz difraktometresi (XRD) analizi sonuçlara göre kalsit başlıca karbonat minerali olarak belirlenmiştir. Bu mineralin, dikitin büyüme ekseni boyunca sert ve massif tabakaların oluşumuna neden olduğu sonucuna varılmıştır. Bu mineral uzun ve eşboyutlu şekiller sergilemekte ve bazı katmanlarında sıvı kapanımlar bulunmaktadır. Az miktarlardaki demir oksit, kil mineralleri ve aragonit gözenekli doku ile birlikte yapraksı tabakalar oluşturmakta ve kalsit tabakaları ile dönüşümlü olarak bulunmaktadırlar. Bu özellikler paleoiklim ve paleoçevresel değişimlerden kaynaklanan hiyatuslara karşılık gelmektedir.

Oksijen-karbon duraylı izotop analizleri ile dikitin büyüme ekseni boyunca elde edilen δ ^{13}C and ve δ ^{18}O ölçümlerindeki değişimler hemen hemen eşdeğişken olup ufak geçişler sergilemektedirler. δ ^{18}O ve δ ^{13}C değerleri sırasıyla, -3.27‰ ve -4.74‰ ile -2.13‰ ve -5.44‰ değerleri arasındadır. Daha zenginleşmiş δ ^{18}O değerleri ılıman ve kuru iklim ile çevrede C4 (mera) tipi bitkilerin varlığını göstermektedir. Diğer taraftan $\delta^{18}O$ oranı sıfırlandığı zaman daha ılık ve nemli iklim ile çevrede C3 (orman) tipi bitkilerin varlığını işaret etmektedir. Dikit örneğinde δ ^{18}O oranlarında ufak değişimler belirlenmiş olup, yapılan ölçümler önemli iklimsel tersinimlerin varlığını göstermemiştir.

Anahtar Kelimeler: Dikit, Paleoiklim, Paleoçevre, Karain Mağarası, Antalya

I dedicate this thesis to my beloved son Alper Türkmenoğlu and say that the important thing is to never stop questioning.

Albert Einstein

ACKNOWLEDGMENTS

The author wishes to express his deepest gratitude to his supervisor Prof. Dr. Gülay Ertaş and Prof. Dr. Emine Saltık for her guidance, advice, criticism, encouragement and insight throughout this thesis.

The author would also like to thank Prof. Dr. Harun Taşkıran for his permission to conduct this research related to Karain Cave, Antalya, and for giving the stalagmite sample for the studies. I have benefited from his valuable suggestions and comments.

I wish to thank my examining committee member, Prof. Dr. Kaan Sayıt for sharing his valuable recommendations and critiques with me.

I am very grateful to Prof. Dr. Asuman Günal Türkmenoğlu for her help during petrographic analysis of thin-sections. I am thankful and very much appreciate the guidance of Dr. Ezgi Ünal İmer for providing a connection with the Radiogenic Isotope Facility at the School of Earth Sciences, The University of Queensland, Australia, to carry out the stable isotope analysis. I would like to express my deepest gratitude to Dr. Selin Süer who performed the stable isotope analysis at the Central Laboratory, METU. I also thank Pelin Paşabeyoğlu who did the XRD analysis at the Central Laboratory, METU. I owe Dr. İbrahim Çam many thanks for his kind help and guidance during the SEM-EDX analysis at the Central Laboratory, METU.

The technical assistance of Mr. Orhan Karaman from the Department of Geological Engineering, METU, is gratefully acknowledged for preparing the thin- sections.

Last but not least, I would like to express my deepest love and gratitude to my dear family who supported me throughout this study.

TABLE OF CONTENTS

ABSTRACT v

ÖZ vii

ACKNOWLEDGMENTS x

TABLE OF CONTENTS xi

LIST OF TABLES xii

LIST OF FIGURES xiii

CHAPTERS

1 INTRODUCTION 1

2 MATERIALS AND METHODS 21

3 RESULTS OF THE STUDY 33

4 DISCUSSIONS 49

5 CONCLUSIONS 53

REFERENCES 55

APPENDICES

LIST OF TABLES

TABLES

Table 2.1 Description of the sampling location of the Karain cave in this study....23
Table 2.2 Locations of the different samples for analysis collected from the Stalagmite Sample. 24
Table 3.1 . Weight percentages of elements in EDX samples. See Appendix A for complete EDX analysis results....40
Table 3.2 The results of δ 13C and δ 18O analysis (in ‰) 44
Table 3.3 Results of U-Th dating of stalagmite sample 48

LIST OF FIGURES

FIGURES

Figure 1.1. Different types of karst landforms. 3
Figure 1.2. . a) Google map showing the location of the Karain Cave b) the entrance to the Karain cave opened within the karstic limestones of Çadır Hill 6
Figure 1.3. Karain cave map showing the positions of the various cavities in the Karain Cave. 9
Figure 1.4. Archaeological levels (AH-5 to 22) of Karain E-Cave. 10
Figure 1.5. Alternating warm and cool periods in the Earth's paleoclimate, deduced from oxygen isotope data derived from deep sea core samples. 11
Figure 1.6. Karain-E correlation between geologic layers and archeological layers. 12
Figure 1.7. Türkiye Palentological chronology. 14
Figure 2.1. Sketch of the Karain Cave, indicating the position of the grid where the stalagmite sample was collected. 23
Figure 2.2. a) The cross-section of the stalagmite sample and the orientation of the thin section sampling areas along the longitudinal direction of the stalagmite sample. The drill holes on the left side of the stalagmite sample show the sampling locations for stable isotope analysis, b) Sampling locations for XRD analysis (Sample No.1a, 1b, 2a, 2b, 3a, 4a, 5). 26
Figure 2.3. Samples have been collected for SEM-EDX analysis. 28
Figure 2.4. Powder samples in sample containers. 29
Figure 3.1. XRD spectra of the samples (as shown in Figure 2.2) showing the characteristic reflections belonging calcite. 34
Figure 3.2. Thin-section photographs of stalagmite sample; a) coarse and elongate calcite (red) crystals (x4, XPL), b) equant calcite (red) crystals associated with iron-oxides (or organic matter) (blue) and pores (green) (x4, PPL), c) thin laminations of half -spherulitic aggregates of calcite, alternating with equant calcite crystals (outlined in the figure in red). Clay accumulations (purple) are

distinguished by brown colored laminae and pores (x4, XPL); d) fluid inclusions (fl) in coarse and columnar calcite (x4, PPL), e) closer view of the fluid inclusions in coarse and columnar calcite (red) (x20, PPL). The basal part of the stalagmite sample; f) lamination characteristic with half-spherulitic aggregates of calcite and bone (orange) fragments (x4, PPL), g) fossil (orange) and bone fragment in micritic matrix (x4, XPL), h) bone fragments (orange), quartz (black) crystal in a clay and micritic matrix (x4, XPL). 35
Figure 3.3. SEM images showing mineral textures and micromorphologies; a) equant calcite crystals(red) with dissolution pits, b) calcite crystals exhibiting rhombohedral cleavage, c) needlelike crystals of aragonite(blue) with square terminations, enclosed by equant calcite crystals(red), d) close view of aragonite (blue) crystals in Fig.6c, e) randomly oriented, bladed/platy aragonite(blue) crystals associated with calcite(red), f) blded aragonite (blue) crystals forming bundles g, h) clay aggregates (purple) in the stalagmite sample. 38
Figure 3.4. SEM-EDX analysis of stalagmite samples. a) the image of equant calcite crystal, b) EDX analysis (No.1.6) of the calcite crystal shown in (a), c) the image of detrital clay deposit in association with calcite minerals, d) EDX analysis (No.2.6) of the clay material. 42
Figure 3.5. Variations in isotope values along the growth axis of the stalagmite sample. Th/U ages of the three samples are also plotted on the diagram. Dashed lines represent 5 groups of fluctuations in δ O/ δ C values. 46

CHAPTER 1

INTRODUCTION

The earth's history involved complex biochemical, geological and climatic changes during its evolution resulting in its present geography and climate. Specialists from different disciplines like geology, biology, chemistry, geophysics, anthropology and archaeology have involved increasingly in palaeoclimatological studies to understand the effects of climate change on earth's ecosystems and human evolution.[1–3] Evidences of the climate changes of the past are preserved in paleoclimate archives of climate data. The archives are natural materials of the earth, such as sediments, fossil shells, tree rings, ice cores, trapped air, speleothems, fluid inclusions, corals, and other archives, that can be sampled and analyzed by a wide variety of physical, chemical and biological methods. They are found widespread everywhere, like in caves, trees, soils etc. Proxies in paleoclimatology are chemical, biological or physical measurements made in many archives including speleothems, ice cores and corals. They serve as essential tools for the reconstruction of climate-related parameters like temperature and vegetation. Stable-isotope ratios of oxygen ($^{18}O/^{16}O$) and carbon ($^{13}C/^{12}C$) are important proxy methods to obtain parameters related to past climates.[1]

Dating and correlation methods are used by researchers to determine the age of geological and biological archives Radiometric dating methods rely on the decay rate of unstable isotopes that are present in naturally occurring elements found in samples which are unique to each element. Their age is determined by measuring the age of the radioactive isotopes in the material. The age being determined is that of the radioactive isotopes and not necessarily that of the material itself. However, external

factors as changes in the production rate in the atmosphere or global and regional reservoir effects can affect the accuracy of the dating analysis, so calibration studies must be conducted to account for such changes.[1]

Speleothems are secondary mineral deposits that form within caves in karstic carbonate terranes. In such environments carbon dioxide gas ($CO_{2(g)}$) is incorporated into water to form carbonic acid (H_2CO_3). The dissolution of carbonate bedrocks by this weak acid occurs according to the following reactions:[4]

$$H_2O + CO_2 \leftrightarrow H_2CO_3$$
$$CaCO_3 + H_2CO_3 \leftrightarrow Ca^{2+} + 2HCO_3^-$$

When percolating water with sufficient dissolved Ca^{2+} and high concentrations of bicarbonate is exposed to the low pCO_2 cave atmosphere, $CaCO_3$ deposition of new carbonate minerals occurs:

$$Ca^{2+} + 2HCO_3^- \rightarrow CaCO_3(s) + H_2O + CO_{2(g)}$$

Speleothems are different than the primary mineral bodies, such as the bedrock of the cave and sediments accumulated in the cave. The primary minerals are important sources of material from which speleothems can grow as a result of physical and chemical processes occurring within the cave[5]. Cave deposits may contain various types of landforms such as stalagmites, stalactites, flow stones, pool deposits and others (Figure 1.1).[6]

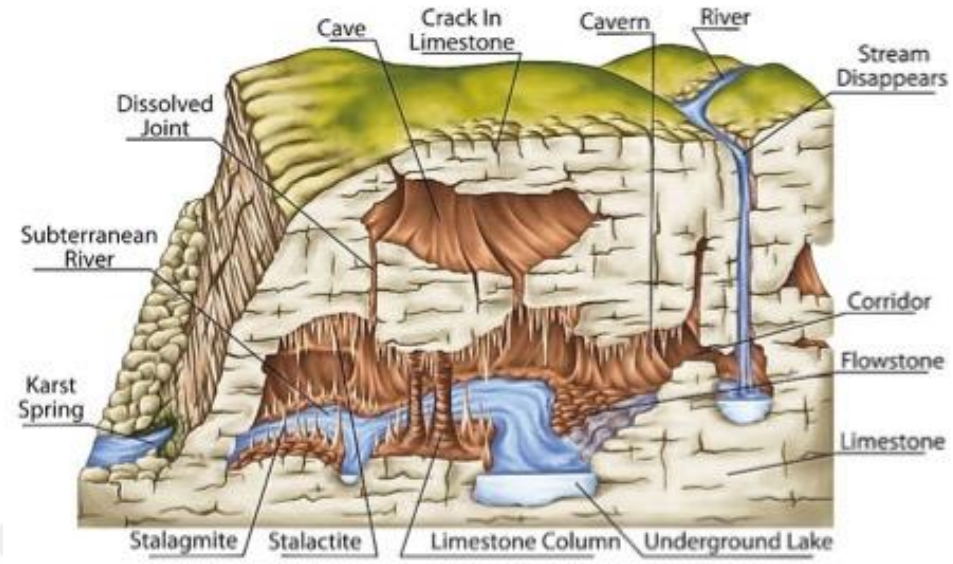


Figure 1.1. Different types of karst landforms.

Caves from karstic terranes may include different minerals, mainly low-magnesium calcite, dolomite and aragonite.[7] During the growth of speleothems, mineralogical oscillations between the mineral precipitates may indicate environmental alternations in the past. The Mg/Ca ratio of both dripping waters and percolating pore fluids, partial pressure of CO_2 (pCO_2), cave atmosphere and its evaporative conditions are the major factors controlling the mineralogical compositions of the speleothems: Low-magnesium calcite (0.5 and 7.5 mol% $CaCO_3$) is a stable mineral in the fresh-water (low (<1 ratio) Mg/Ca), low-temperature environment. On the contrary, dolomite (35 and 50 mol% $MgCO_3$) precipitation occurs from solutions enriched in Mg due to drier climatic conditions and as a result of a prior crystallization of low-magnesium calcite. Cave air pCO_2 (carbon dioxide partial pressure) is, along with drip rate, one of the most important factors controlling speleothem carbonate precipitation. Consequently, pCO_2 has an indirect but important control on speleothem proxy data (e.g., elemental concentrations, isotopic values). Rain waters and percolating waters in the cave environment adsorb CO_2 from the soil and karstic carbonate rocks, to form carbonic acid. On reaching the open space of the caves, the solutions are supersaturated in CO_2 with respect to the

cave atmosphere. The deposition of carbonate minerals occurs as a result of CO_2 degassing.

In paleoclimatologic investigations in cave environments, speleothems have the potential to provide a continuous record of climate change over a long period through analysis of their mineralogy, petrography and geochemistry and thus inform if climate was a major contributor towards reconstructing past climates and human evolution.[8] Although different types of speleothems (Figure 1.1) are widespread in karstic cave environments, stalagmites are the major paleoclimate archive used to reconstruct past climates and continental paleo-environments because of their well-defined stratigraphic order and suitability for obtaining measurements for climate sensitive stable isotope (oxygen and carbon) signals and radiometric age determinations.[9–11]

Caves are the most famous example of shelters during the Paleolithic age, which corresponds with the Pleistocene epoch of the Quaternary period in the geological time scale. The Paleolithic age was lasted from about 2.6 million to the beginning of Holocene epoch of the Quaternary at around 11,600 BP, and is characterized by the world's most recent period of repeated glaciation.[12] Paleolithic human populations were hunter -gatherers who made tools using stones, bones, wood and similar materials, while finding shelter in caves and other rock shelters. Caves often preserve archeological evidence of extended periods of human occupations. In Anatolia, caves have been surveyed intensely and Karain cave above the Antalya plain was discovered by Prof. Dr. İ. Kılıç Kökten near Yağca village.[13] Since then archaeological investigations have been continued, proving that the Karain cave in Antalya area is one of the best site reflecting the cultural sequence of Paleolithic and Epipaleolithic ages in Anatolia and is the only Paleolithic site for establishment of the Paleolithic Chronology of Turkey.[14–16] To date, important information on the cultural evolution, human evolution and ecological environment of Paleolithic populations lived in and around the Karain cave were obtained by the studies of

archives mainly as stone tools, faunal remains, bones, raw material sources and the infill sediment deposits.[17,18] However, there are few studies on the past climate changes recorded by Karain cave deposits as exemplified by Djerrab and Aïfa[19] who studied the effects of various magnetic parameters on climatic changes during the infilling history of the Karain Cave. Rink and coworkers[20] measured ages using teeth samples from archaeological soil levels using Electron Spin Resonance (ESR) and dated these teeth samples back to last interglacial warm phases (e.g., Greeenland Interglacials). Yalçınkaya and coworkers[21] studied the 6 meter thick sedimentary sand and clay deposits filling the E-cavity of the Karain Cave. They identified six stratigraphic units which were correlated with specific archaeological units. U/Th radiometric dating of minerals extracted from layer sediments by using Electron Spinning Resonance (ESR) method assigned precise ages for each layer within a time range of 70,000 to 44,000 years. The stratigraphic units were found to be correlated with different climatic stages.

It is known that analyses of speleothem formations provide valuable climate proxy data for evaluating climate changes occurring at glacial-interglacial transitions. Stalagmites are useful sources of paleoclimate information since they respond rapidly to climate variations[22] and they can be dated precisely using various age dating methods such as U-Th dating, ESR dating, Thermo Luminescence (TL) dating and stable isotope geochemistry dating techniques.[11,23–25] Although stalagmite samples unearthed during the archaeological excavations at Karain Cave, there has been no paleoclimate studies carried out by means of archaeometric methods, yet.

The aim of this study is to analyze a stalagmite sample from the Karain Cave using of petrographic microscope, scanning electron microscope (SEM-EDX), X-ray powder diffraction (XRD), stable isotope (oxygen and carbon) and U/Th radiometric age dating techniques in order to determine, first the mineralogical, textural, micromorphological and geochemical characteristics of the stalagmite and their variation along its growth axis, secondly to make interpretation for variations in the

local microenvironment and changes of the climatic conditions in the case site by the correlation of the proxy parameters obtained from the stalagmite.

1.1 Location and the Geographic and Geologic Setting of the Study Area

The Karain Cave complex composed of many connected cavities is situated approximately 30 km northwest of Antalya, close to Yağca village, on the slopes of Katran mountains (Beydağları Massif of western Taurus) as shown in Figure 1.2 (a). It is easily reachable by car from Antalya by taking the road D650 to Burdur and after exiting to the west along Karain Street. The cave is opened within the limestone cliffs of the Çadır Hill as shown in Figure 1.2 (b) it is 430-450 m above sea level. The entrance to the cave is located about 150 meters above the Antalya's coastal travertine plain. [26]



(a)

Figure 1.2. . a) Google map showing the location of the Karain Cave b) the entrance to the Karain cave opened within the karstic limestones of Çadır Hill

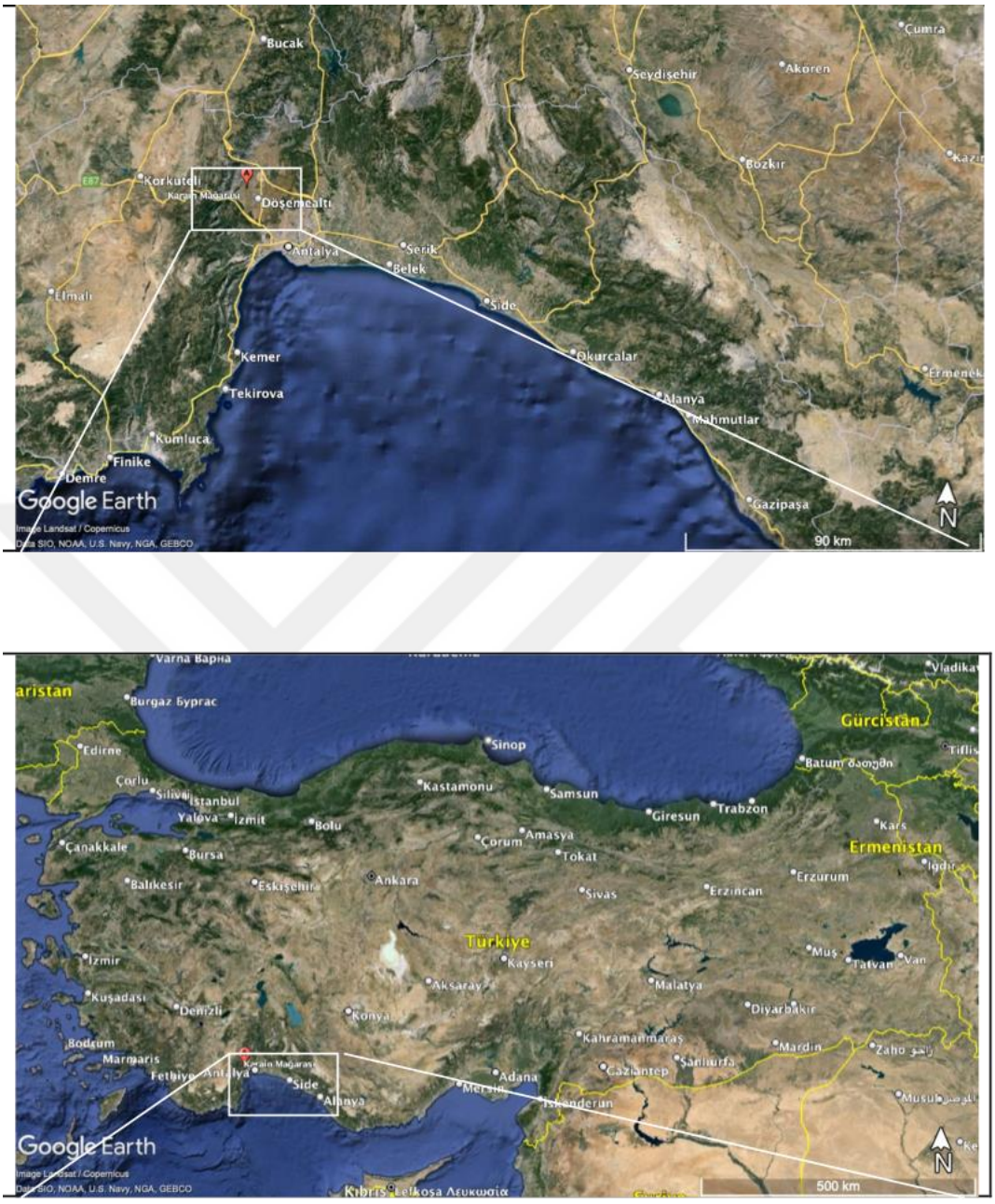


Figure 1.2. . a) Google map showing the location of the Karain Cave b) the entrance to the Karain cave opened within the karstic limestones of Çadır Hill (continued)



Photgraph taken from https://turkisharchaeonews.net/site/karain-cave

(b)

Figure 1.2. . a) Google map showing the location of the Karain Cave b) the entrance to the Karain cave opened within the karstic limestones of Çadır Hill (continued)

Although the climate of the Mediterranean region is generally dry and warm during summers and is characterized by mild winters. The specific geomorphological characteristics of the local areas may present climate differences compared to nearby regions.[17]

Geographically, the environment around the Karain Cave is evolved by tectonic movements, faults, hydrologic processes and climate. It is characterized by two completely different geomorphological landscapes: the first one is represented by high relief mountains (Katran mountains) with the highest hill elevated about 1450 meters above sea level. The thick marine carbonate sequence of these mountains was deposited during the Mesozoic age in the Neo-Tethyan oceanic basin. Later on, tectonic uplifting formed these high relief mountains due to mountain building processes of the Alpine orogeny. Hydrogeological processes took place during Pliocene-Pleistocene (from 5Ma to around 11,600 BP) leading to the karstification of limestones and the formation of the slopes cut by short valleys, deep canyons, high ridges and cave systems. The second characteristic landscape form is the coastal Antalya plain which corresponds to Holocene marine bays. It is 50 km wide and

continuous 25 km inland towards mountains and the elevation in land increases within a short distance, abruptly from sea level to around 1 km. [27,28] Antalya plain consists of 3 plateau surfaces, the uppermost one is the Döşemealtı tufa surface. Humans occupied caves and rock shelters at the Katran mountains above the Döşemealtı plateau during the Paleolithic and Neolithic times.[17]

Topographical plan view of Karain cave showing various cavities, drawn on the topographical studies. They are named as A to G (Figure 1.3).[14]



Figure 1.3. Karain cave map showing the positions of the various cavities in the Karain Cave.

1.2 Previous Studies

In this section previous studies are summarized to demonstrate the relation of this study to past work which bears directly on the problems to be attacked in the present investigation. They were discussed under two subtopics as follows.

Kökten[13] reported his survey studies on the Anatolian Prehistoric sites. He plotted these sites on a map showing widespread distribution of rock shelters, caves, mounds, Paleolithic to Neolithic artefacts, fortress and flintstone quarries etc. He

located for the first time Karain cave near Yağca village and found stone tools indicating a Paleolithic settlement in this area.

Rink and coworkers[20] obtained ESR ages on 18 teeth from archaeological levels AH16-AH27 (see Figure 1.4) in the cavity-E at Karain Cave.[14]

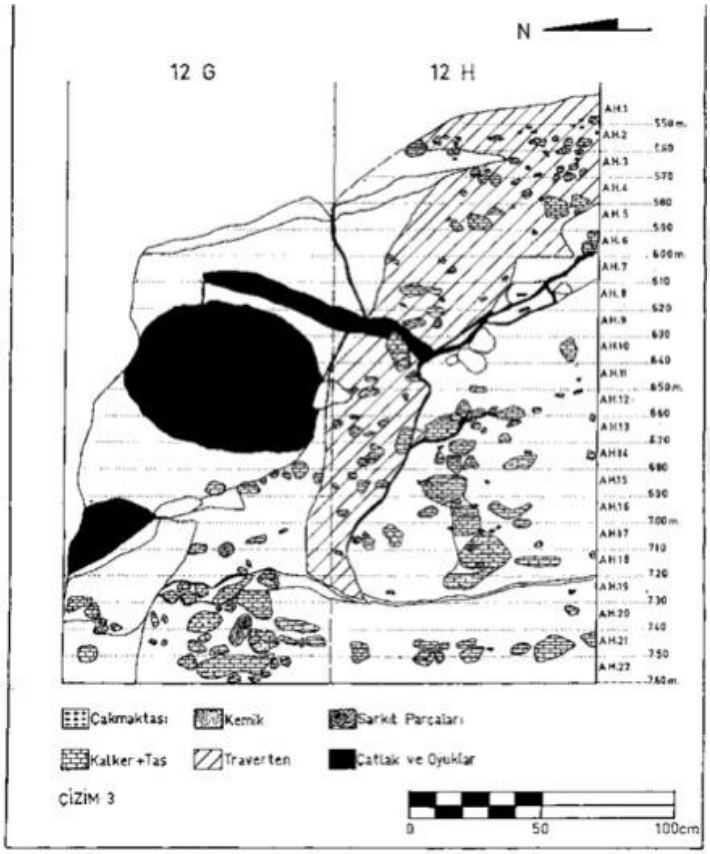


Figure 1.4. Archaeological levels (AH-5 to 22) of Karain E-Cave.

This sequence exhibited a transition in lithic assemblage from a technological characteristic of lithic stones Classic Charentian (797k to 347k years BP eg.) to a Karain (Zagros-type) Mousterian (60 to 70 k years BP) between levels AH27 and AH25, and two calcite-cemented soils at levels AH22 and AH16 which have been interpreted as climatic warm phases. They assigned this sequence a mean early

uptake (EU) age of 108 ± 23 ka and mean linear uptake (LU) age of 121 ± 27 ka. Based on the ESR dating results, they concluded that deposition of the two different lithic assemblages and both the penultimate and the final climatic warm phases at Karain most probably occurred during oxygen isotope stage 5 which are Marine isotope stages (MIS), marine oxygen-isotope stages, or oxygen isotope stages (OIS), are alternating warm and cool periods in the Earth's paleoclimate, deduced from oxygen isotope data derived from deep sea core samples as seen in Figure 1.5.[29]

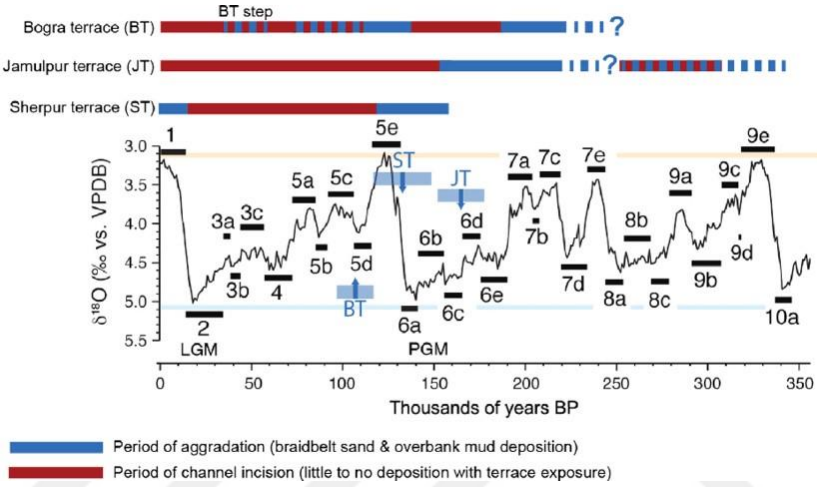


Figure 1.5. Alternating warm and cool periods in the Earth's paleoclimate, deduced from oxygen isotope data derived from deep sea core samples.

Another conclusion was that these lithic assemblages were significantly different than contemporaneous Levantine Mousterian industries which occurred about 700 km to the southeast of Karain Cave.

Yalçınkaya and coworkers[30] summarized the Karain excavations continued between 1985-1995 with an emphasis on the importance of the Anatolian Paleolithic ages. Up to date results of the sediment analysis combined with the U-series ages were used to establish a correlation chart for the Karain E-cavity showing the relations between dates obtained by U/Th and ESR methods; $^{16}O/\ ^{18}O$ ratios; geological layers; archaeological unites; technical characteristics (thickness of the flakes, bladelets, microliths, discoidal, etc.) and lithics (obsidian, chert, limestone etc.) tools. The general stratigraphic unit (geological layer) “I” matched with the last Glacial Age

(European Würm) dated approximately 60,000-70,000 BP. In this way a paleoclimatologic information could be obtained for archaeologic stratigraphy of the E-cavity. This data on the Paleolithic chronology of the Karain cave points out the importance of the studies of human migration along the Levantine corridor (Figure 1.6).[30]

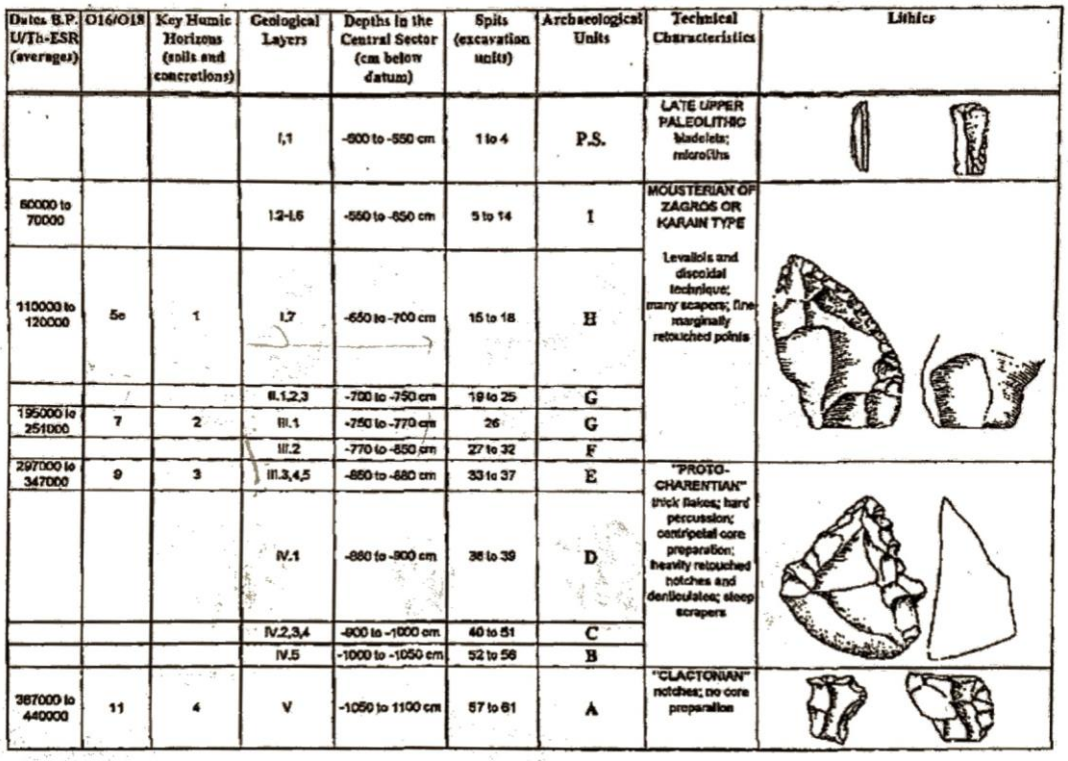


Figure 1.6. Karain-E correlation between geologic layers and archeological layers.

Djerrab and Aïfa[19] investigated the relation of rock magnetism to stratigraphy and palaeoenvironment of the Karain E-cavity infill. The magnetic properties were compared with the sedimentological study. The sediments of this site showed a period of ca. 500 ka and belonged to the Middle and Upper Pleistocene. They concluded that the evolution of the magnetic parameters was in accordance with climatic changes that took place during the infilling history of the cave. The clayey levels indicated a humid climate and favored the formation of secondary iron oxides at the top of the infill, i.e. in Level 6.

Yaman[18] studied sedimentology and chipped stone artefacts found in Karain cave and investigated the connections especially between Middle Paleozoic archaeologic stratigraphies of the B and E- cavities. Additional methodology applied consisted of mineralogical thin- section analysis of the sediments, their X-ray powder diffraction and chemical analysis proved to be useful for correlation purposes.

Thin section and XRD analysis have shown that the sediments found in the geological layers of both cavities have similar mineralogical compositions. They both contain quartz, biotite, calcite and limestone and chert fragments. The sediments of E cavity are believed to have come from eolian (wind transported) sources, in addition to the travertine type cave deposits. XRF analysis has showed that the two geological levels are chemically similar, which makes it possible to correlation between the E and B cavities. Further studies of the chipstone technology characteristics during the Middle Palaeozoic chipstone have indicated that the Zagros Type Mousterien (or Karain Type Mousterien) and Charentien industries are characteristic for the E cavity. On the other hand, only the Zagros Type Mousterien industry is defined for B cavity. These cultural remains are attributed to Homo Neanderthalensis, as this human species occupied the Karain Cave during the Middle Palaeozoic.

Taşkıran[16,31] prepared comprehensive review of the Paleolithic and Epi-paleolithic of Anatolia. He summarized the excavation studies of the Karain cave since its discovery by Prof. Dr. İ.Kılıç Kökten in 1946. He explained the crucial role of the cave in forming the Paleolithic chronology of Anatolia (Figure 1.7). There was a continuous settlement during the Late Neolithic, Chalcolithic, Early Bronze Age and Roman Periods which makes Karain cave significant for world.

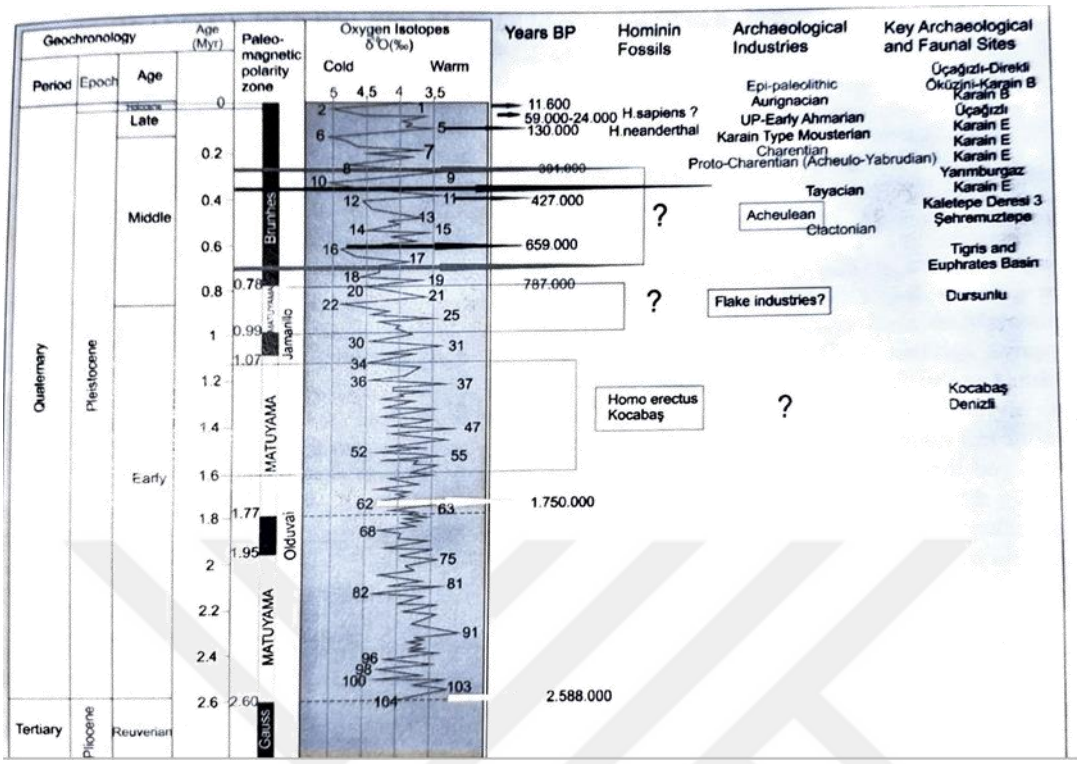


Figure 1.7. Türkiye Palentological chronology.

Koşun and coworkers describes origin, karstification processes of plateaus, and their geologic ages in detail.[17] Karstification is a geological process that takes place when carbonated rocks such as limestone and dolomite, are exposed to leaching caused by tectonic uplift at the Earth's surface. This leaching is often caused by streams and results in the formation of unique landforms such as caves, sinkholes, springs and underground streams. The isotopic ages and flora contents of Antalya Tufa indicated that the middle and lower plateaus were formed during the Würmian regression period. The Würm glaciation stage was the last glacial period in the Alpine region covering a time period between 115,000 to 11,700 years ago. This stage terminated with the beginning of Holocene which is the current geological epoch. They explained in detail the importance of the Antalya Plain for the Mediterranean and European prehistory. The excavations in Karain proved a continuous cultural and technological evolution from Lower Paleolithic (1 Ma to 300 ka) towards Holocene

(>11.4 Ka) and corresponding chipped stone industry and human species such as Homo Eractus, Homo Neanderthalensis and Homo Sapiens.

Kuzucuoğlu and coworkers explained in detail the geomorphological characteristics and major landscapes of Antalya region from the points of view of the geographic and structural context.[27] Landscapes are characterized by high relief formed by carbonate series and widespread coastal plain consisting of Antalya travertine (tufas), Pliocene conglomerate and Plio-Quaternary plain fill. These landforms were formed by combined effects of tectonic, faulting, hydrological processes and climate as in the case of karstic landforms provided settlement sites, such as the Karain Cave, for human species during prehistoric times.

1.3 Karain Cave and Previous Archaeological Investigations

Bar-Mathews and coworkers discussed the environmental controls such as cave atmosphere, water compositions, their Mg/Ca ratio, isotope ratios, temperature and evaporation of speleothem mineralogy in a karstic dolomitic terrane, Soreq Cave, Israel.[32] Speleothems were characterized by two mineralogic types, the first as low Mg-calcite and the second variety as low Mg-calcite alternating with high Mg-calcite. Mineralogical oscillations between low Mg-calcite and Mg-enriched composite zones may indicate environmental alternations in the past. They concluded that mineralogical and petrographic studies of speleothems could provide evidence of paleoclimatic change. Laminated speleothems can undergo mineralogical oscillations with varying O and C isotope compositions. These changes may indicate evaporation or a shift in vegetation type. During periods of climatic change such as glacial-interglacial, or grassification in dry periods, internal changes within the cave may result in the dissolution and precipitation of carbonates with different isotopic compositions. These changes can be identified through detailed mineralogic and petrographic analysis.

Self and Hill used mineralogic techniques to use speleothems.[33] By the ontogeny technique individual crystals and their aggregates were studied as physical as bodies rather than mineral species. This paper introduced the basic principles of this subject and explained a hierarchy scheme whereby mineral bodies can be studied as crystal individuals, aggregates of individuals, associations of aggregate and as sequences of ensembles.

The detailed structure and texture of speleothems can be examined through microscopic examination of thin sections and by using a Scanning Electron Microscope. Some examples of textural include spherulites which have either a radial or curving radial structure due to the splitting of crystals and dendritic (tree like) structures that have a branching pattern due to crystal splitting. In caves, dendritic crystals usually form in the high evaporation conditions of a capillary film environment. The ontogeny of minerals is a method by which past crystallization environments can be interpreted from the mineral bodies that were deposited. The structure and texture of minor mineral bodies can be directly related to environmental factors.

White prepared a review for characteristics and application of cave sediments as paleoclimate archives.[34] Cave sediments could form either stream-transported clastic sediments or calcite speleothems, both of which were useful for climatic records. The techniques used for dating cave sediments were radiocarbon and U/Th dating of speleothems, paleomagnetic reversals and cosmogenic isotope dating of clastic sediments. Isotope and trace element profiles, color banding and luminescence profiles of mainly stalagmites, produced paleoclimate records over the past several hundred thousand years. The author concluded that these methods can be applied to late Holocene climates for evaluation of current concern over global warming.

Erkan studied stalagmites collected from 15 caves located in and around the Konya Closed Basin in order to reconstruct the paleoclimate in central Anatolia.[35] Stable isotope analysis (oxygen and carbon) and Th/U age dating revealed that, in general, the current climate regime in central Anatolia was established after the Early

Holocene. The climate was in less humid and cool mode until the Holocene and changed to a more humid and warmer regime during the Holocene period. Spötl and Boch summarized the methods for cavers, speleologists, and other interested individuals to determine the age and growth of speleothems.[23] One of the commonly used techniques is the ^{14}C which provides only a rough estimate of the formation age of speleothems. Additionally, this method can only date samples up to approximately 50,000 years old. The uranium-thorium (U/Th) dating method was first applied to speleothems in the early 1970s and since then, it has undergone dramatic improvements. One of the advantages of this method is that it can provide U/Th ages at high precision, up to per-mil level However, impurities in the sample remain a common problem. Although various approaches exist to correct for the nonradiogenic Th fraction, they are all based on assumptions resulting in larger age uncertainties. U-series dating of speleothems is among the most highly respected chronological techniques, providing time information for studies of the environment and climate of the past.

Duan and coworkers studied the mineral composition and structure of the stalagmite laminae from a cave in India using XRD and SEM and their significances for paleoclimatic reconstruction.[36] Stalagmite was found mainly composed of primary aragonite. The growth of alternation of compact/porous aragonite sub-layers might be formed in different seasons. It was emphasized that it was important to analyze the mineralogy and structure of stalagmite laminae for explaining paleoclimate changes.

Erdoğu and coworkers studied speleothem samples including stalagmites from Çatalhöyük and caves around this area to find their original locations.[37] Elemental composition of these samples was determined using ICP-MS and. U-series (U-Th) dating was carried out using a thermal ionization mass spectrometer (TIMS) to find similarities between the Çatalhöyük samples and speleothem deposits from surrounding caves based on similarities between their ages and their mineral compositions. They reported that the Çatalhöyük's speleothems were transported

from caves in southern and eastern parts of Çatalhöyük at a distance of about 100 km.

Perrin and coworkers reported a process-based approach combining mineralogical, textural, and geochemical data to characterize diagenetic processes shown by aragonite and calcite speleothems.[38] There was growth interruption and inclusion levels indicating discontinuous growth of stalagmites in this cave. Recrystallization processes included textural change of original aragonite precipitates and two distinct types of aragonite-to-calcite recrystallization. The recrystallization of aragonite-to-calcite causes Mg enrichment and Sr depletion in calcite. For this reason, only the primary calcite and primary aragonite have high potential for preservation of paleoclimatologic signal. U/Th dating is possible only for both primary calcite and aragonite in speleothems. These results proved the potential importance of studying diagenetic processes affecting stalagmites used in paleoclimatic interpretation.

Watanabe and coworkers studied for dating a cylindrical fragment of stalagmite from Caverna do Diabo, Brazil, using thermoluminescence (TL) and electron paramagnetic resonance (EPR) techniques.[39] XRD pattern of the stalagmite sample indicated that the sample consists of pure calcite. The age of the samples (labeled as slices 1, 2 and 3) obtained by EPR method were comparable to the value obtained by TL measurements. The average age of the central part of stalagmite was found to be 86,410 years. The coherence of the dating by TL and EPR techniques and the presence of rings indicated that the stalagmite can be used as a climatic record.

Polyak and coworkers examined Holocene-aged stalagmites that have highly resolved layers to be used for identifying drought and pluvial periods in climate.[10] These stalagmites exhibited annual banding of fluid inclusions that refers to the process of forming layers and bands of fluids within the stalagmite, and aragonite layers and growth hiatuses that represent drier periods. Growth hiatuses were associated with aragonite layers or dark magnesium-rich silicates. This study examined the layer types using grayscale and carbon and oxygen stable isotope time-

series tied to a high-resolution U-series chronology. They reported that the clear calcite layers represent drought, not pluvial, conditions.

Martín-García and coworkers investigated diagenetic transformation of aragonite to calcite and its effect on stable isotope geochemistry and U-series dating.[11] Stalagmite was obtained from a cave in Spain. The diagenetic process included recrystallization to calcite, micritization and dissolution. Additionally, U-leaching and U-loss took place during transformation process during the transformation process. Primary and secondary mineral phases had an impact on geochemical information.

This method has been widely used in combination with other geochemical analyses (major and minor elements, stable isotopes, etc.) to obtain paleoclimate information. However, in some cases, U/Th analysis indicates inverted ages for speleothem layers, which would seem to disqualify the dating since the acceptance of an age as correct is based on its accordance with stratigraphic order. However, in some cases, U (or Th) remobilization could indicate that there has been remobilization of other chemical species as well, and so transformed aragonite to calcite speleothems should be treated with caution.

The studied stalagmite is composed of both aragonite and calcite. Scanning Electron Microscope observations were carried out to determine all mineralogies and textures. Concentrations of Ca, Mg, Sr, Fe, Mn and Ba including all mineralogies and textures were determined by using an Electron Microprobe Analyzer. Samples for stable isotopes were collected along the central growth axis of the stalagmite at increments of 0.25 to 0.5 mm, and 73 transversal from the core to the surface at increments of 0.25 mm. Powders were then analyzed on a GV2003 continuous-flow isotope ratio mass spectrometer. Stable carbon and oxygen isotopic ratios are reported in ‰, relative to the Vienna Pee Dee Belemnite (VPDB) and the Standard Mean Ocean Water (SMOW) scales using the standard notation.

Observations with petrographic microscope and SEM showed dissolution of primary columnar aragonite crystals which transform into needle like aragonite crystals. Elemental analysis determined the distribution of elements in all the different

mineralogies. The amount of Mg^{2+} distinguishes aragonite from calcite where aragonite have ~0% mol $MgCO_3$ for the large calcite crystals $MgCO_3$ reaching up to 1.07 in the smaller crystals indicating that the difference in Mg^{2+} concentration can distinguish between calcite and primary aragonite and, thus forms evidence of a primary mineralogical phase. O and C isotopic values change both along the growth axis and perpendicular to the axis. For example, in the aragonite rim of the speleothem, both $\delta^{13}C$ and $\delta^{18}O$ values are heavier than in the calcites, particularly with $\delta^{13}C$, which reaches up to −6.04‰ VPDB. In order to provide a time frame for the diagenetic processes affecting the samples. U-series dating on seven points selected along the vertical growth axis and including all the fabrics identified by optical microscopy were carried out to provide a time frame for the diagenetic processes affecting the samples. Comparing these results with the stratigraphic observations and the diagenetic path, there were some inconsistencies. At the lowermost stratigraphic level along the growth axis, calcite (age: ±76.3240.8 ka) that transforms the primary aragonite is older than the aragonite (age: 49.7820.6 ka) itself. Whereas aragonite (age: 195.351 ± 2.1 ka) of the tip-uppermost level along the growth axis is the oldest in the speleothem.

The results show that during transformation, the system stayed close in one of the stages, and open in the other, with the same textural result. Reverse ages are found either in the recrystallized areas or in the primary aragonite caused by different U-remobilization mechanisms, U-leaching due to flowing waters on the surface, and U-loss during the transformation process. These results highlight the complex behavior of speleothems during diagenesis and the impact on the geochemical information of the primary and secondary phases. Thus, the importance of petrological and geochemical characterization of speleothems for paleoclimatic studies cannot be overstated.

CHAPTER 2

MATERIALS AND METHODS

2.1 Description of the Stalagmite Sample

Stalagmites are often studied in caves to understand paleoclimatic conditions and paleo-ecological environments. The most widely measured isotope ratios during stalagmite research are focused on $^{18}O/^{16}O$ and $^{13}C/^{12}C$. The oxygen isotope ratio is related to temperature and is widely interpreted as a paleoclimate thermometer. The carbon isotope ratio is associated with the type of vegetation on the land surface above and has been used to distinguish variation in vegetation as forest from grassland.[34]

Stalagmite growth in karstic caves occurs gradually from calcite ($CaCO_3$) precipitated from cave drip water. Stalagmites contain important information that helps to understand paleoclimatic records. The ratio of stable isotopes within the calcite, particularly the ratio of ^{18}O to ^{16}O (shown also as $\delta^{18}O$) is used for this purpose. Stalagmite $\delta^{18}O$ is supplied by drip water, which is rainwater circulating through karstic limestone bedrock and soil. The oxygen isotope ratio of rainwater is primarily affected by temperature and the $\delta^{18}O$ of water from its source region. Therefore, stalagmites record changes in these water isotope parameters. These factors make stalagmites a focus of studies using $\delta^{18}O$ for paleotemperature reconstruction in cave environments. Chronological data obtained by U-series age dating also contributes to the understanding of climatic evolution of the environment.[22,40]

Cave carbonate deposits such as stalagmites are valuable sources of information about ecological environments and climate. The ratio between ^{13}C to ^{12}C ratio (also shown as $\delta^{13}C$) can indicate the type of vegetation present which reflects changes in precipitation, temperature and other factors. The carbon isotope variations in stalagmites are related with $\delta^{13}C$ values of atmospheric CO_2 dissolved in rainfall, as well as the CO_2 released by plant respiration and the decomposition of soil organic matter.[41]

In Karain Cave, the Lower Paleolithic layers of the E-cavity are represented by the geologic units V and VI, the latter being stratigraphically older. The geologic unit V includes a number of archaeological levels described between 53-59.[42]

The lithologic and archaeostratigraphic characteristics and artefacts unearthed from this unit during the excavations from the different sections of the E-cavity were described according to their grain size (sand and clay), color (grey and dark brown) and presence of carbonate concretions by Yalçınkaya and coworkers.[15,21,43–45]

Stalagmites are commonly found in the Karain cave deposit and are often associated with hard carbonate layers containing concretions.[45] Stalagmite samples were gathered and are currently being stored in the excavation storehouse for further analysis using archaeometric methods.

The stalagmite sample studied during in this thesis study was provided by Prof. Dr. Harun Taşkıran and it belongs to the E-cavity of Karain Cave. The sample is located in the Grid/archaeolevels marked as J17/55-60 as shown in Figüre 2.1. Unit V, which included the stalagmite sample, correlates with these archaeolevels and is referred to as the geological (archaeostratigraphic) unit The elevation measurements of the top and bottom boundaries (codes) of unit V are -10.75 m and -11.18 m, respectively, indicating a layer thickness of 43 cm as listed in Table 2.1.[46] This geologic unit consisted of sediments deposited during Early Palaeolithic period in the Karain cave ranging in age between 1Ma-300 ka.[17]

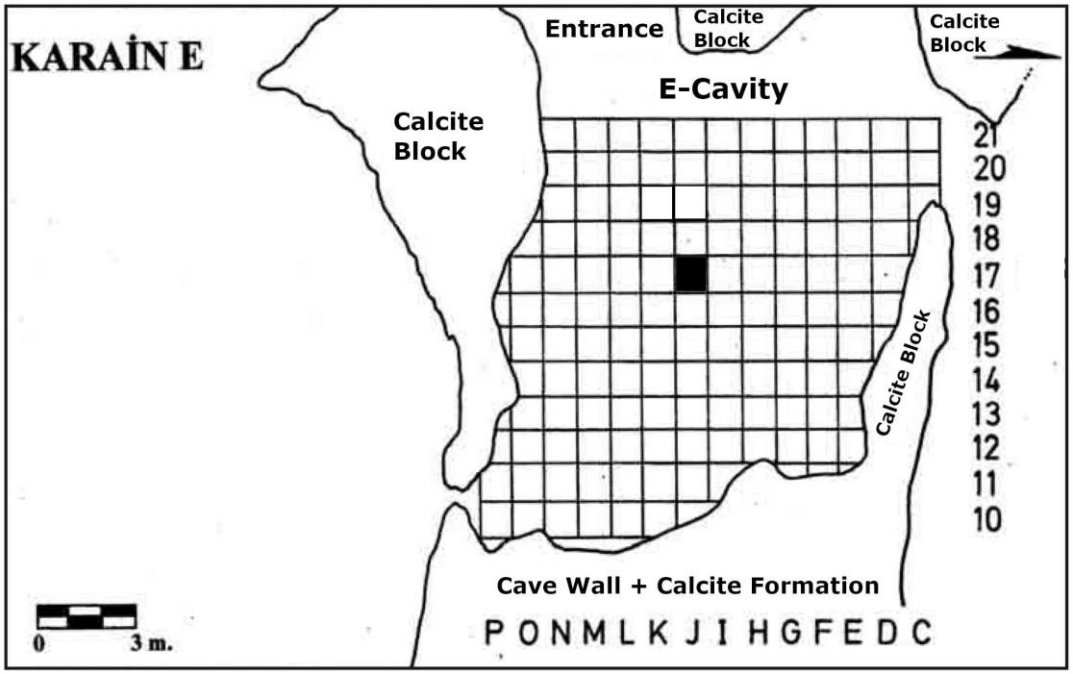


Figure 2.1. Sketch of the Karain Cave, indicating the position of the grid where the stalagmite sample was collected.

Table 2.1 Description of the sampling location of the Karain cave in this study.

Grid	Archaeologic level	Geologic unit	Top code of the unit (m)	Bottom code of the unit(m)
J17	**55-60**	**V**	**-10.75**	**-11.18**

Thin section, SEM-EDX, XRD, Th-U and Stable Isotope Sample location colleced from the stalagmite is given in Table 2.2.

Table 2.2 Locations of the different samples for analysis collected from the Stalagmite Sample.

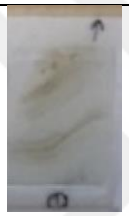
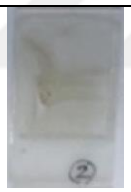
Sample height (mm) From top to bottom	Thin section samples	SEM-EDX Samples	XRD Samples	Th-U Samples	Stable Isotope Samples
0 to 33		1	 1a and 1b	KR5 (5 mm)	KR0 to KR32
33 to 66		2	 2a and 2b		KR34 to KR66
66 to 99			 3	KR79 (79 mm)	KR66 to KR99
99 to 130			 4	KR130 (130 mm)	KR99 to KR130

Table 2.2 Locations of the different samples for analysis collected from the Stalagmite Sample (continued)

From bedrock 0 to -33			 5		
From Bedrock -33 to -66					

The picture of stalagmite sample and sampling areas for thin section and XRD analysis are shown in Figure 2.2. The stalagmite sample has a conical shape and a carbonate sequence of 130 mm along its longitudinal axis (Figure 2.2a).



(a)



(b)

Figure 2.2. a) The cross-section of the stalagmite sample and the orientation of the thin section sampling areas along the longitudinal direction of the stalagmite sample. The drill holes on the left side of the stalagmite sample show the sampling locations for stable isotope analysis, b) Sampling locations for XRD analysis (Sample No.1a, 1b, 2a, 2b, 3a, 4a, 5).

At the Rock Mechanics Laboratory of the Mining Engineering Department of METU, the sample was cut into two equal pieces longitudinally using a diamond saw. The stalagmite base consists of transported deposits such as angular shaped carbonate rock fragments within a matrix of brown clay and macroscopic organic fragments. In the upward direction, a stalagmite forms with wavy layers of carbonate

and clay deposits. Voids resulting from the dissolution of carbonate material are observable along some laminations. Yalçınkaya and coworkers state that stalagmites in the E-cavity of the Karain cave formed during wet seasons, indicating hydrological changes in the cave based on the fact that carbonate dissolution forming voids require water flow and this indicates rainy seasons effecting the layers with voids.[43,47] This also means that layers which do not contain voids correspond to dry seasons.

2.2 Thin -Section Analysis

Through the analysis of petrographic thin-sections, the mineralogical compositions and textural characteristics of the stalagmite sample were identified Six successive thin sections were prepared in a longitudinal direction along the vertical growth axis of the stalagmite at the Thin-section Laboratory of the Geological Engineering Department of METU as shown in Fig.2.2a.

A thin slice of the sample was cut with a diamond saw. It is then mounted on a glass slide using a Canada Balsam resin and ground with a diamond impregnated wheel. It was polished to a thickness of 30 μm using carborundum grit and water on a lapping machine, gradually using finer grits. Then, to protect the thin- sections cover glass was placed over them.[48] The thin-section samples were analyzed with an Olympus CX31 model petrographic microscope and images were captured using Olympus BH2 Model petrographic microscope and a Nikon Coolpix 995 camera.

2.3 Scanning Electron Microscopy (SEM)

The SEM analysis was conducted at the Central Laboratory of METU. Two samples from the stalagmite were analyzed using a high resolution (able to distinguish details of a specimen at a minimum distance of 1.2 nm) QUANTA 400F Field Emission scanning electron microscope (SEM) coupled with an energy dispersive X-ray spectroscopy (EDX). The freshly broken surfaces of Sample 1 and 2 as depicted in

Figure 2.2b were coated with carbon to ensure electron conductivity of the surfaces Samples were chosen visually from the pure section of the stalagmite (**Error! Reference source not found.**). The SEM analysis aimed to identify minerals based on their micro and nanoscale morphologies, while the EDX analysis helped identify crystals by obtaining their elemental compositions.



Figure 2.3. Samples have been collected for SEM-EDX analysis.

2.4 X-Ray Powder Diffraction (XRD)

Seven powder samples (Sample No. 1a, 1b, 2a, 2b, 3a, 4a, 5) were collected using a Dremel Stylo+hand drill. The samples were taken from different layers along the longitudinal direction of the vertical growth axis of the stalagmite, as shown in Figure 2.2b. The drill bits used were 0.8-2.0 mm in size. Powder samples were collected parallel to the longitudinal axis of the stalagmite. The sampling interval for the stable isotope analyses was 1.0-2.0 mm, depending on the growth rate of the

stalagmite. Each sample weighed approximately 0.1 g and was collected to a depth of about 1 mm. Samples collected from each longitudinal point were mixed and placed in sample containers, as shown in Figure 2.4.

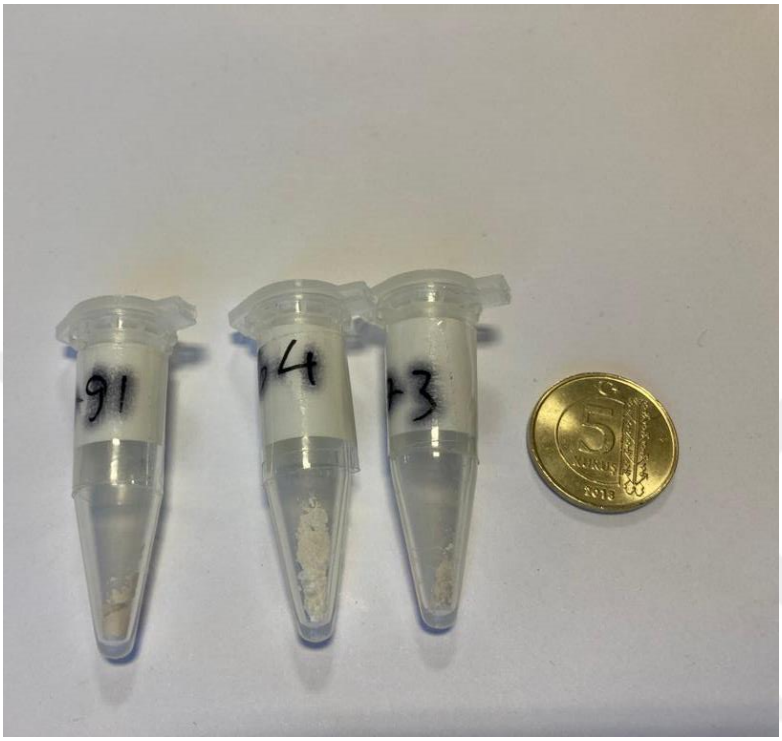


Figure 2.4. Powder samples in sample containers.

Once the sample was collected from each longitudinal point, the drill bit was cleaned with ethyl alcohol to remove any contamination. XRD measurements were performed on these powdered samples using a Rigaku Ultima-IV powder diffractometer at the Central Laboratory of METU to identify the mineral composition using bulk powder samples. The samples were scanned in the 2-60°2Θ range using Cu K_α radiation and a scanning speed of 2°/min.

2.5 Stable Isotope Analysis

$\delta^{13}C$ and $\delta^{18}O$ isotope ratios of 95 carbonate samples taken from the stalagmite were identified using the Gas Bench-Continuous Flow Isotope Ratio Mass Spectrometry technique. The ThermoFinnigan -DeltaPlus XP Isotope Ratio Mass Spectrometer available at the Central Laboratory of METU was utilized.

Ethanol was used to clean the surface of stalagmite. Powder samples weighing 0.2-0.4 mg were placed into the sample holders and mixed with 0.1 mL Ortho-Phosphoric acid (99%, Merck) at 70°C on an automatic sampling tray for approximately 2 h. The CO_2 gas released by this reaction was purified by an intermediate unit Gas Bench and then sent to the mass spectrometer for separating its isotopes. The ion ratios of CO_2 were converted to raw isotopic ratios by ISODAT software. NBS19 Limestone (NIST) ($\delta^{13}C$: 1.95 ‰ and $\delta^{18}O$: -2.20 ‰) was the major standard used during the analysis and was analyzed together with experimental set of samples. It was used to convert the raw isotope ratios to the real isotopic values, converting radiocarbon isotope ages to calendar year timescales.

The stable isotope ratios (δ) were reported in permil (‰) unit relative to the VPDB which is shorthand for **V**ienna **P**ee **D**ee **B**elemnite. δ values (d values) are calculated by:

$$(\text{in } ‰) = (R_{sample}/R_{standard} - 1)\ 1000$$

where "R" is the ratio of the heavy to light isotope in the sample or standard.[49]

2.6 U-Th Radiometric Age Dating Analysis

Geochronological analyses were carried out at the Radiogenic Isotope Facility at the School of Earth Sciences at The University of Queensland. Australia. U-series isotopic analyses were carried out on a Nu Instruments multi-collector inductively coupled plasma-mass spectrometer (MC-ICP-MS). Three carbonate samples, selected for maximum possible purity by visual inspection were collected from a

stalagmite using Dremel Stylo+ hand drill bits (0.8-2.0 mm size) at depths of 5 mm (KR-005), 79 mm (KR-079) and 130 mm (KR-130) depths from the top towards the bottom of the sample. Ethanol was used to clean the surface of stalagmite during sampling. The U-Th ages were calculated using the Isoplot 3.75 Program of Ludwig.[49]Two standards Yarrangobilly flowstone stock, YB-1 (an Australian National University speleothem standard with an age of 30.2±0.6 ka and Harwell Uraninite, HU-1 which is a commonly used Uraninite standard with known ages were used in calibration.

CHAPTER 3

RESULTS OF THE STUDY

3.1 Results of the Mineralogical and Petrographical Studies

A stalagmite is a type of cave deposit formation that develops from water dripping in a cave. As minerals precipitate, they create alternating layers along the growth direction visible in hand specimens. The major carbonate minerals forming layers include low-magnesium calcite ($(Ca_{0.998},Mg_{0.002})CO_3$), dolomite ($CaMg(CO_3)_2$), aragonite (a polymorph of $CaCO_3$) and rarer carbonates such as huntite ($Mg_3Ca(CO_3)_4$), vaterite (a polymorph of $CaCO_3$), and nesquehonite ($Mg(HCO_3)(OH)•2(H_2O)$).[7] Mineralogical controls are mainly the Mg/Ca ratio of percolating pore-fluids, pCO_2, and evaporative conditions within the cave.[32] Detrital minerals like clay minerals may also be deposited in the form of laminations. Well-laminated stalagmites are a valuable tool for reconstructing past climate changes based on their mineralogy, petrography and textural properties.[36] Therefore, it is important to investigate these properties in detail using different research techniques.

The stalagmite sample studied in this thesis exhibits various laminations and layers which can be differentiated visually by their color, compactness and porosity as shown in Figure 2.2a. The colors vary between white, dirty white and brown which is caused by the accumulation of dust or clay. The Compact layers are white with higher hardness and are non-porous.

In this section, the results of the thin-section analysis, SEM and XRD analyses will be reported. All these methods used complement each other and help to correctly identify minerals and their compositional, textural and micromorphological properties.

As explained in Section 2.2, continuous thin sections of a stalagmite sample were prepared along its longitudinal axis to study mineralogical and petrographical characteristics. Using a petrographic microscope and XRD as shown in Figure 3.1, calcite was identified as the main carbonate mineral. The most characteristic reflections of calcite corresponded to d-spacing values (Å) of 3.86, 3.04, 2.50, 2.29 and 2.10.[50,51]

Weaker intensity reflections of calcite were also measured. In thin sections, we observed different morphologies of calcite crystals. The coarse and columnar calcite crystals have elongated shapes and are long axis oriented subparallel to the growth direction of the stalagmite, forming compact and thicker layers. These crystals showed twinning under crossed polars. Another variety was equant and grainy calcite crystals of variable sizes, which could associate with iron oxide along the laminations, including pores, as shown in Figure 3.2b. The third morphological variety of calcite formation was restricted to thin laminations, characterized by half-spherulitic aggregates of calcite as shown in Figure 3.2c. These laminations could alternate with small-sized equant calcite layers.

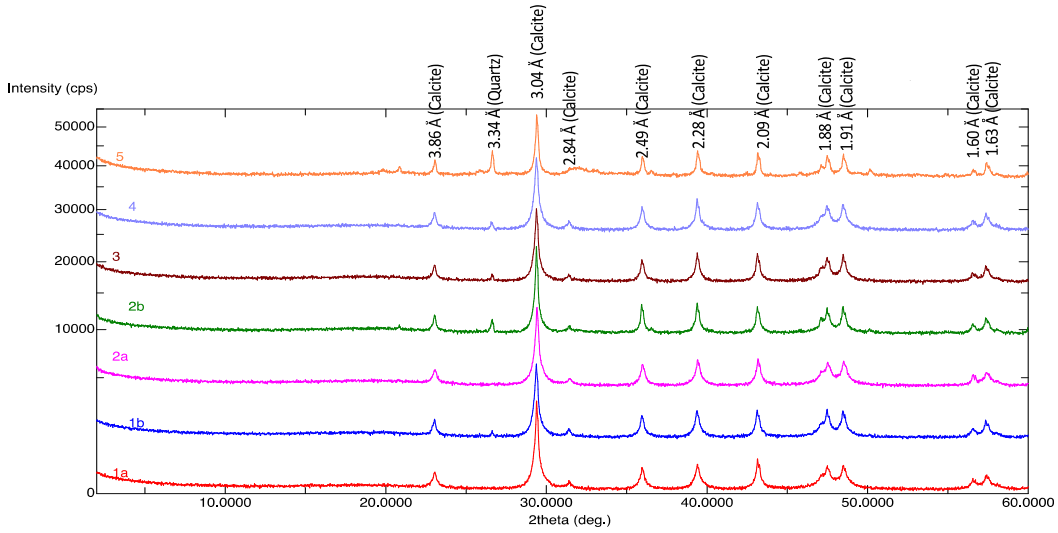


Figure 3.1. XRD spectra of the samples (as shown in Figure 2.2) showing the characteristic reflections belonging calcite.

The stalagmite sample has coarse and columnar calcite crystals in compact and thicker layers. These crystals have elongated shapes and contain fluid inclusions as seen in Figure 3.2d, e. These inclusions are believed to be trapped drip waters from which the stalagmite precipitated.[31,52] The bottom part of the stalagmite sample (Figure 2.2a) consists of a lamination characteristic with half-spherulitic aggregates of calcite (Figure 3.2f), fossils, bone fragments in a matrix of clay and micritic calcite (Figure 3.2 g, h).

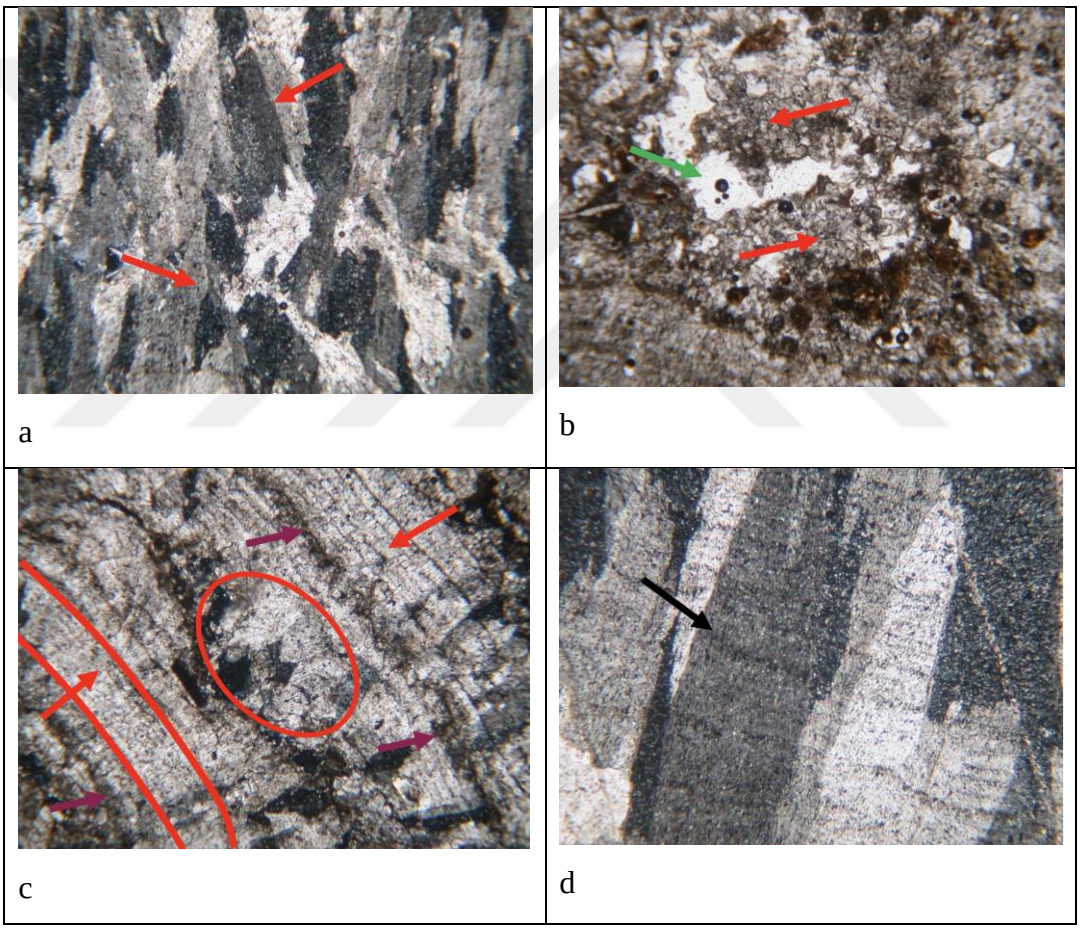


Figure 3.2. Thin-section photographs of stalagmite sample; a) coarse and elongate calcite (red) crystals (x4, XPL), b) equant calcite (red) crystals associated with iron-oxides (or organic matter) (blue) and pores (green) (x4, PPL), c) thin laminations of

half -spherulitic aggregates of calcite, alternating with equant calcite crystals (outlined in the figure in red). Clay accumulations (purple) are distinguished by brown colored laminae and pores (x4, XPL); d) fluid inclusions (fl) in coarse and columnar calcite (x4, PPL), e) closer view of the fluid inclusions in coarse and columnar calcite (red) (x20, PPL). The basal part of the stalagmite sample; f) lamination characteristic with half-spherulitic aggregates of calcite and bone (orange) fragments (x4, PPL), g) fossil (orange) and bone fragment in micritic matrix (x4, XPL), h) bone fragments (orange), quartz (black) crystal in a clay and micritic matrix (x4, XPL).

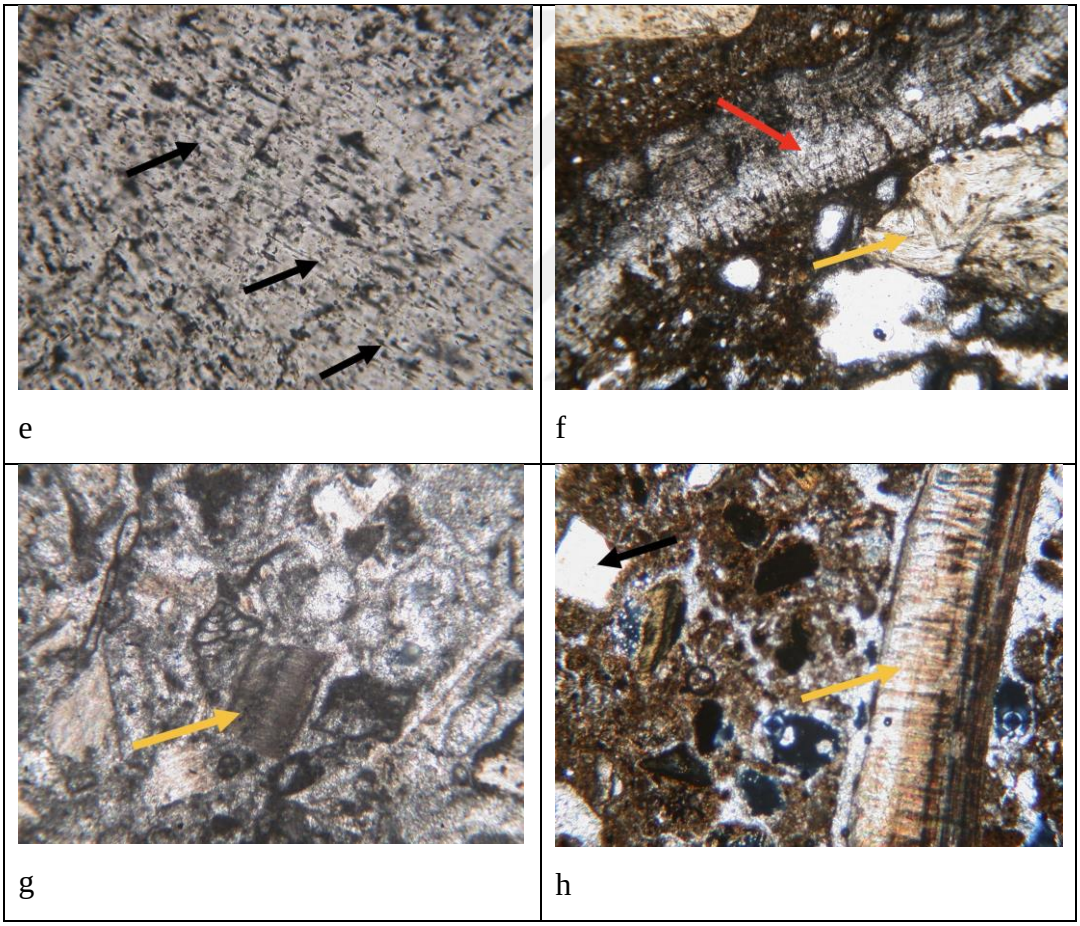


Figure 3.2. Thin-section photographs of stalagmite sample; a) coarse and elongate calcite (red) crystals (x4, XPL), b) equant calcite (red) crystals associated with iron-oxides (or organic matter) (blue) and pores (green) (x4, PPL), c) thin laminations of

half -spherulitic aggregates of calcite, alternating with equant calcite crystals (outlined in the figure in red). Clay accumulations (purple) are distinguished by brown colored laminae and pores (x4, XPL); d) fluid inclusions (fl) in coarse and columnar calcite (x4, PPL), e) closer view of the fluid inclusions in coarse and columnar calcite (red) (x20, PPL). The basal part of the stalagmite sample; f) lamination characteristic with half-spherulitic aggregates of calcite and bone (orange) fragments (x4, PPL), g) fossil (orange) and bone fragment in micritic matrix (x4, XPL), h) bone fragments (orange), quartz (black) crystal in a clay and micritic matrix (x4, XPL). (continued)

SEM analysis coupled with EDX analysis was useful in identifying minerals, observing textures and micromorphologies in detail. SEM images showing mineral textures and micromorphologies are given in Figure 3.3. The calcite crystals in the sample are grainy with random orientation. Cleavage planes and a few dissolution pits formed due to the weathering of stalagmite can be observed (Figure 3.3a). Elongate calcite crystals have a rhombohedral cleavages shape and are commonly found in speleotherms, as shown in Figure 3.3b. According to Bar-Matthews and coworkers, this textural form is frequently observed in speleothems and shows enhanced supersaturation and growth rate.[32] We did not detect any aragonite, which is a polymorph of calcite, in the studied samples using the petrographic microscope and XRD, because its quantities were low. However, aragonite can be identified through SEM analysis as needle-like crystals with square terminations as seen in Figure 3.3c,d or as bladed/platy crystals with random orientations (Figure 3.3e) or as bundles (Figure 3.3f). Aragonite is found to have close associations with calcite and appears to be its secondary alteration product.[38] Additionally clay aggregates were observed in the stalagmite sample, as shown in Figures 3.3g and 3.3h.

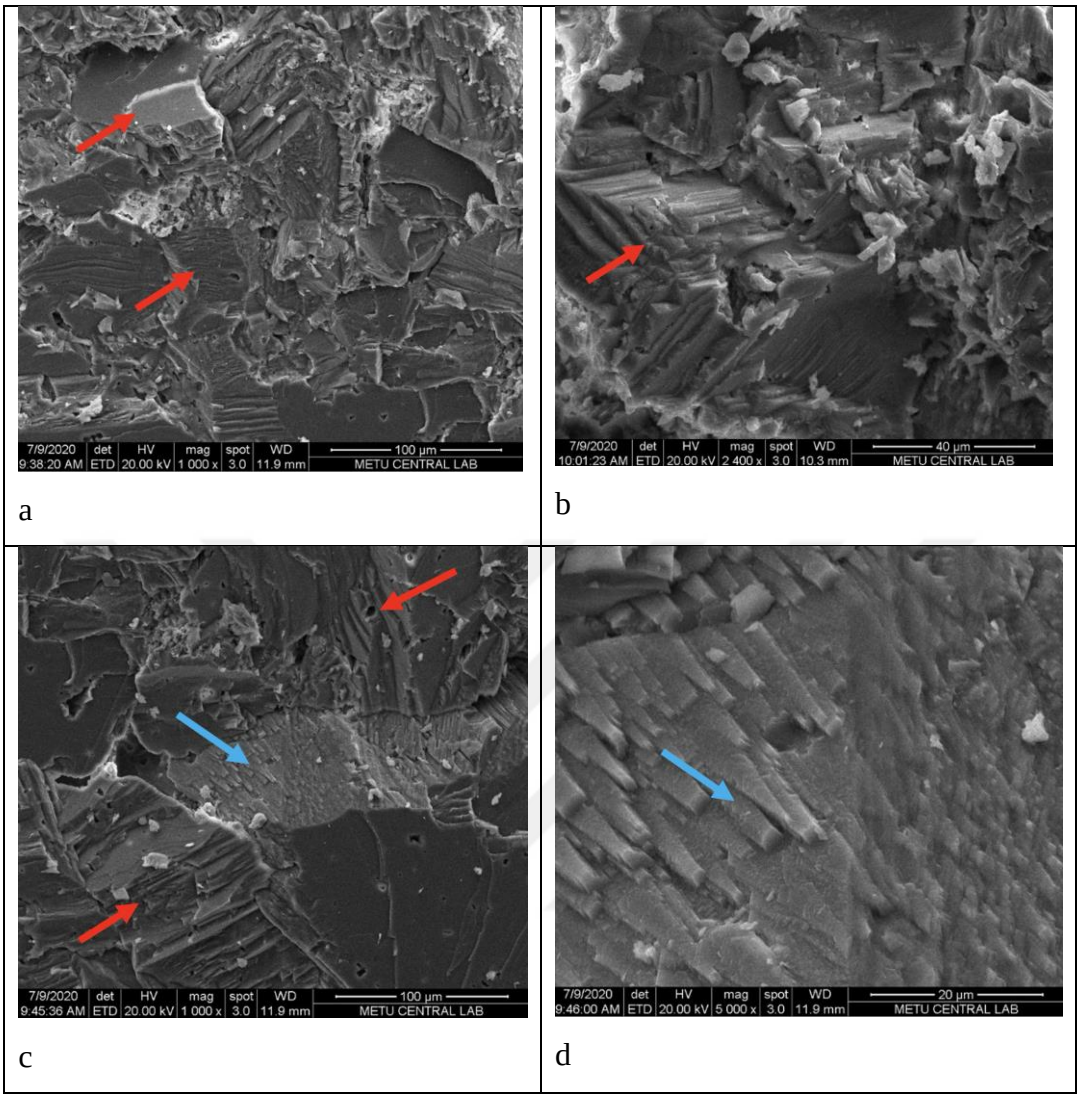


Figure 3.3. SEM images showing mineral textures and micromorphologies; a) equant calcite crystals(red) with dissolution pits, b) calcite crystals exhibiting rhombohedral cleavage, c) needlelike crystals of aragonite(blue) with square terminations, enclosed by equant calcite crystals(red), d) close view of aragonite (blue) crystals in Fig.6c, e) randomly oriented, bladed/platy aragonite(blue) crystals associated with calcite(red), f) blded aragonite (blue) crystals forming bundles g, h) clay aggregates (purple) in the stalagmite sample.

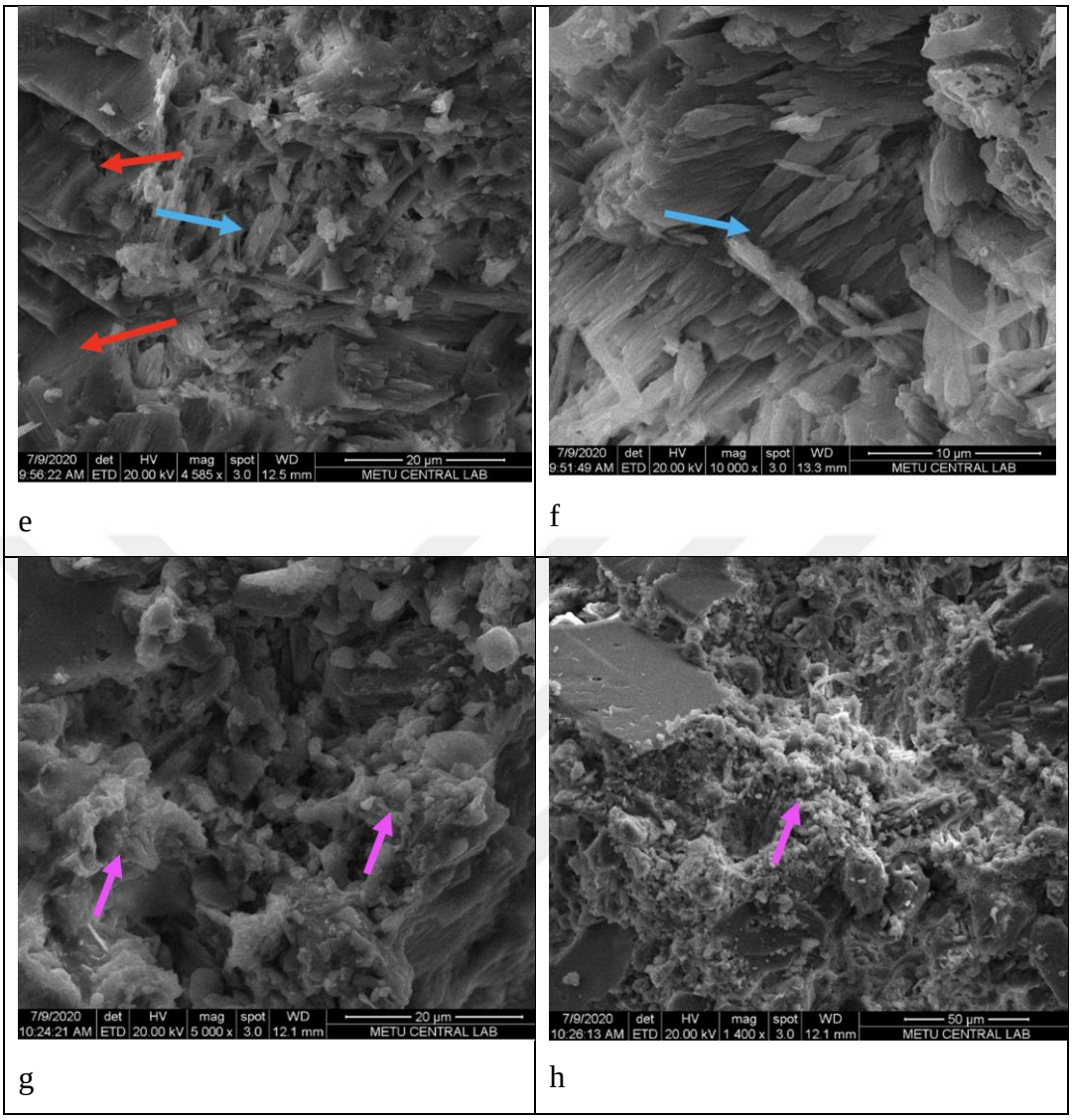


Figure 3.3. SEM images showing mineral textures and micromorphologies; a) equant calcite crystals(red) with dissolution pits, b) calcite crystals exhibiting rhombohedral cleavage, c) needlelike crystals of aragonite(blue) with square terminations, enclosed by equant calcite crystals(red), d) close view of aragonite (blue) crystals in Fig.6c, e) randomly oriented, bladed/platy aragonite(blue) crystals associated with calcite(red), f) blded aragonite (blue) crystals forming bundles g, h) clay aggregates (purple) in the stalagmite sample. (continued)

SEM studies were conducted on a stalagmite sample, and EDX analysis revealed the presence of calcite and silicate minerals (clay minerals) in these samples. The concentration of elements in weight percentages is listed in Table 3.1. The weight percentages of elements in eight analyses (No.1.3;1.4;1.5;1.6;1.7; 1.9; 2.2 and 2.3) showed that Mg, P, K and Fe were not detected. This indicates almost pure calcite (Figures 3.4 a, b). The other four analyses (No. 2.6; 2.9; 2.10 and 2.11) detected Mg, P, K and Fe in the sample. Except for No. 2.10, all these analyses indicated relatively higher quantities of Al and Si. Additionally, the analyses numbers 2.6 and 2.9 detected P and Fe and Mg and K, although in very small quantities. This shows the existence of a detrital clay component associated with the calcite mineral (Figure 3.4c, d). The presence of P might be due to its adsorption by accumulated clay minerals from the dripping waters in the cave environment.

Table 3.1 . Weight percentages of elements in EDX samples. See Appendix A for complete EDX analysis results

Element	**1.3***	**1.4***	**1.5***	**1.6***	**1.7***	**1.9***
C	13.2	13.3	14.5	19.	12.08	14.65
O	37.8	35.1	37.4	41.98	33.52	37.51
Al	1.07	**1.65**	0.79	0.75	0.94	0.89
Si	1.91	**3.14**	1.21	0.55	1.97	1.75
Ca	45.9	46.9	46.2	37.38	51.49	45.21
Mg	-	-	-	-	-	-
P	-	-	-	-	-	-
K	-	-	-	-	-	-
Fe	-	-	-	-	-	-
Total	100	10	100	100	100	100

Table 3.1 . Weight percentages of elements in EDX samples. See Appendix A for complete EDX analysis results (continued)

Element	**2.2***	**2.3***	**2.6***	**2.9***	**2.10***	**2.11***
C	19.38	14.53	15.51	13.13	24.38	14.35
O	40.48	35.94	39.58	42.53	48.39	46.31
Al	0.99	0.60	**3.54**	**2.51**	0.39	**3.71**
Si	1.85	0.44	**6.41**	**6.07**	0.38	**5.18**
Ca	37.30	48.49	27.68	30.51	25.45	27.13
Mg	-	-	0.92	0.54	0.29	0.40
P	-	-	**3.20**	**2.05**	0.43	0.82
K	-	-	0.92	0.55	0.29	0.55
Fe	-	-	**2.25**	**2.11**	0.00	1.56
Total	100	100	100	100	100	100

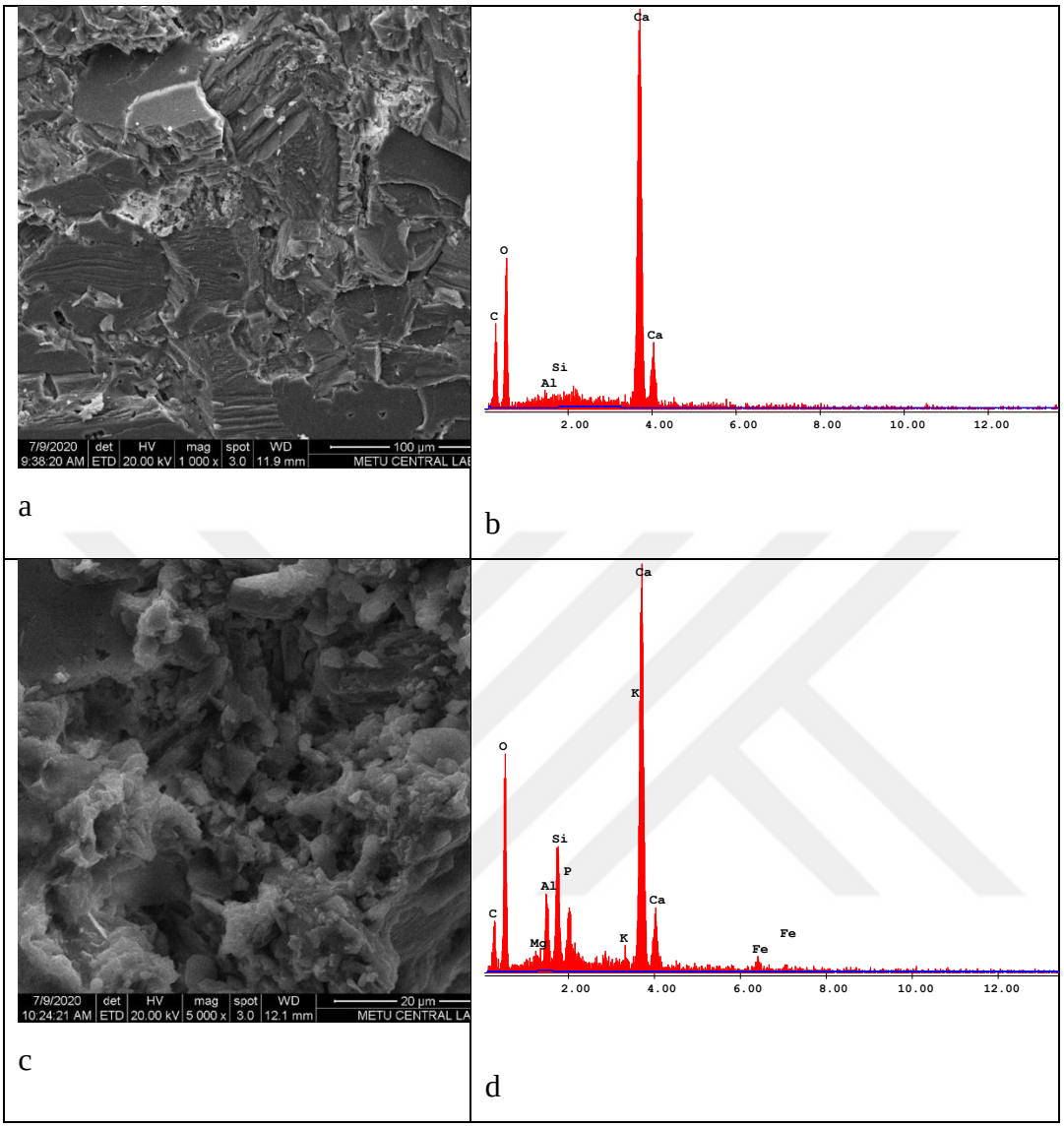


Figure 3.4. SEM-EDX analysis of stalagmite samples. a) the image of equant calcite crystal, b) EDX analysis (No.1.6) of the calcite crystal shown in (a), c) the image of detrital clay deposit in association with calcite minerals, d) EDX analysis (No.2.6) of the clay material.

3.2 Results of the Stable Isotope (Oxygen and Carbon) Studies

Earlier studies have demonstrated that environmental factors such as precipitation and the portion of C3 plants (forests) and C4 plants (grasslands) with different C-cycle pathways have significant impacts on the $\delta^{13}C$ value of soil CO_2.[39] During the cold and dry periods (glacial), karst formation and soil formation were poor as and C4 plants dominated, resulting in heavy $\delta^{13}C$ values (eg. -2 and -3 $\delta^{13}C$ ‰ VPDB). On the contrary, during warm and humid periods (interglacial), C3 vegetation thrived, resulting in more negative $\delta^{13}C$ values (eg. -5 and -6 $\delta^{13}C$ ‰ VPDB). Consequently, the $\delta^{13}C$ values from stalagmites serve as a proxy for changes in vegetation, which is an indirect consequence of climate changes in temperature, precipitation, and other factors.[41]

During this study, stable isotope analysis of oxygen and carbon was conducted on a stalagmite sample from the Karain cave to obtain paleoclimatic and paleo-ecologic parameters. The measurements of the stable isotope ratios ($\delta^{13}C$ and $\delta^{18}O$) of 95 carbonate samples which were collected along the longitudinal growth axis of the stalagmite as explained in Section 2.4, are listed in Table 3.2. The variations in isotope values along the growth axis are plotted in Figure 3.5.

Table 3.2 The results of δ 13C and δ 18O analysis (in ‰)

Sample No	δ ^{13}C(‰) VPDB	δ ^{18}O(‰) VPDB	Height from bottom to top (mm)	Corr ^{230}Th age (ka)
KR130(bottom)	-2.31	-4.17	0	63±22 (Sample No: KR-130)
KR129	-2.36	-4.75	1	
KR128	-2.32	-4.51	2	
KR127	-2.17	-4.44	3	
KR126	-2.15	-4.36	4	
KR123	-2.23	-4.51	7	
KR122	-2.23	-4.37	8	
KR121	-2.20	-4.45	9	
KR120	-2.54	-4.43	10	
KR119	-2.74	-4.45	11	
KR118	-2.89	-4.26	12	
KR117	-2.94	-4.26	13	
KR116	-2.69	-4.2	14	
KR115	-2.7	-4.23	15	
KR114	-2.46	-4.16	16	
KR113	-2.6	-4.4	17	
KR112	-3.14	-4.38	18	
KR111	-2.93	-4.49	19	
KR110	-2.92	-4.42	20	
KR109	-2.69	-4.1	21	
KR107	-2.71	-4.03	23	
KR106	-2.8	-4.09	24	
KR105	-2.87	-4.09	25	
KR104	-2.95	-4.15	26	
KR103	-2.95	-4.16	27	
KR102	-2.85	-4.25	28	
KR101	-2.9	-4.20	29	
KR100	-3.18	-4.34	30	
KR99	-2.79	-4.23	31	
KR98	-3.37	-4.35	32	
KR97	-2.75	-4.45	33	
KR96	-3.44	-4.34	34	
KR95	-3.4	-4.29	35	
KR94	-3.34	-4.15	36	
KR93	-3.81	-4.19	37	
KR92	-3.75	-4.16	38	
KR91	-3.88	-4.05	39	
KR90	-3.85	-4.13	40	
KR89	-3.69	-3.93	41	
KR88	-4.10	-4.08	42	
KR87	-4.20	-4.06	43	
KR86	-4.21	-4.11	44	
KR85	-4.27	-4.03	45	
KR84	-3.91	-3.69	46	
KR83	-3.47	-3.47	47	
KR82	-3.77	-3.52	48	
KR80	-4.76	-3.92	50	
KR79	-5.44	-3.71	51	96±33 (Sample No: KR-79)
KR78	-5.38	-4.1	52	
KR77	-5.36	-4.06	53	
KR76	-4.38	-3.45	54	

Table 3.2 The results of δ 13C and δ 18O analysis (in ‰) (continued)

KR75	-4.14	-3.41	55	
KR74	-4.00	-3.36	56	
KR73	-4.41	-3.56	57	
KR72	-3.84	-3.31	58	
KR71	-4.63	-3.63	59	
KR70	-4.56	-3.65	60	
KR69	-4.26	-3.74	61	
KR68	-4.11	-3.66	62	
KR67	-3.79	-3.68	63	
KR66	-3.53	-3.83	64	
KR65	-3.61	-4.19	65	
KR64	-3.6	-4.17	66	
KR62	-3.43	-4.02	68	
KR60	-3.75	-4.29	70	
KR58	-3.84	-4.44	71	
KR56	-3.99	-4.43	73	
KR54	-3.84	-4.26	75	
KR52	-3.79	-4.19	77	
KR50	-4.18	-4.21	79	
KR48	-4.29	-4.18	81	
KR46	-4.36	-4.21	83	
KR44	-4.44	-4.35	85	
KR42	-4.4	-4.57	87	
KR40	-4.25	-4.18	89	
KR38	-4.76	-4.33	91	
KR36	-4.28	-4.06	93	
KR34	-4.47	-4.15	95	
KR32	-4.54	-4.36	97	
KR30	-4.26	-4.48	99	
KR28	-4.38	-4.56	101	
KR26	-4.27	-4.64	103	
KR24	-4.31	-4.65	107	
KR22	-3.66	-4.08	109	
KR20	-3.69	-3.88	111	
KR18	-3.14	-3.79	113	
KR16	-3.42	-3.86	115	
KR14	-3.14	-3.96	117	
KR12	-3.70	-4.00	119	
KR10	-3.91	-4.13	121	
KR8	-4.34	-4.2	123	
KR6	-3.41	-3.75	125	78±32 (Sample No: KR-005)
KR4	-2.43	-3.33	127	
KR2	-2.13	-3.27	129	
KR0(top)	-0.69	-2.44	131	

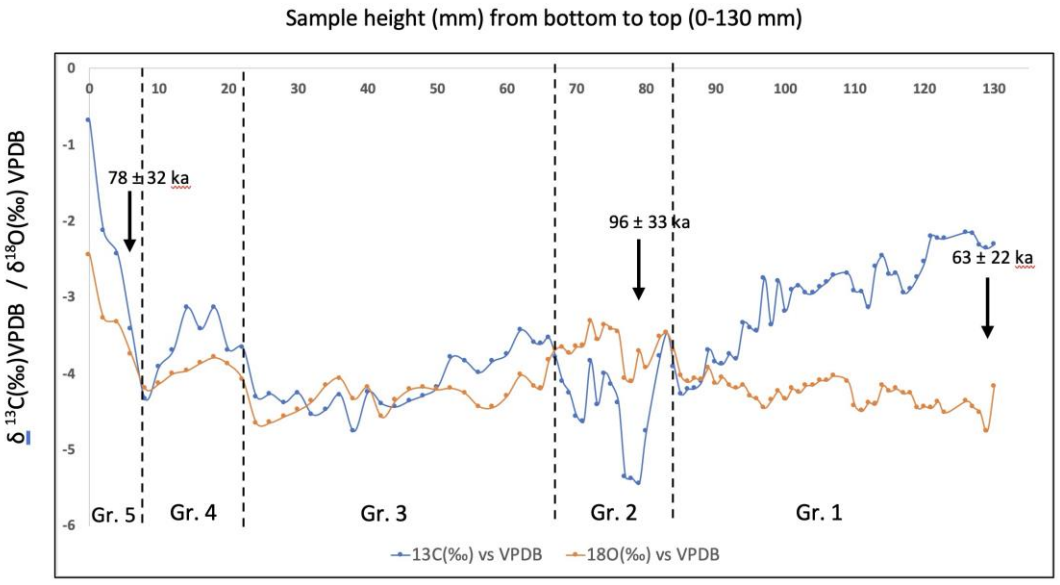


Figure 3.5. Variations in isotope values along the growth axis of the stalagmite sample. Th/U ages of the three samples are also plotted on the diagram. Dashed lines represent 5 groups of fluctuations in δ O/ δ C values.

In Figure 3.5, the δ ^{13}C and δ ^{18}O curves show fluctuations that can be categorized into 5 groups based on the major breaks on δ O/ δ C fluctuations, along the growth axis of the stalagmite from bottom to top (ref. Table 3.2):

Group 1. (130 mm-45 mm). δ ^{13}C values decreasing between -2.31‰ to -4.27‰ ; δ ^{18}O values slightly increasing between -4.17‰ to -3.74‰.

Group 2. (46 mm-62 mm). δ ^{13}C values strongly fluctuates between -3.47 ‰ and -5.44‰ ; δ ^{18}O values range from -3.47‰ and -4.10‰.

Group 3. (63 mm-107 mm). Both δ ^{13}C and δ ^{18}O values decrease: δ^{13}C ranges from -3.43‰ and -4.54‰; δ ^{18}O ranges from -3.63 ‰ and -4.57‰.

Group 4. (109 mm-123 mm). Both δ ^{13}C and δ ^{18}O values increase : δ^{13}C ranges from -3.14‰ and -4.34‰; δ ^{18}O ranges from -3.79 ‰ and -4.20‰.

Group 5. (124 mm-130 mm). Both δ ^{13}C and δ ^{18}O values increase**:** δ^{13}C ranges from -0.69‰ and -3.41‰; δ ^{18}O ranges from-2.44‰ and -3.75‰.

For both isotopes, peak values were observed at their maximum levels for Groups 2 and 4. However, for the other Groups, no drastic changes were measured for $\delta^{13}C$ and $\delta^{18}O$.

3.3 Results of the U-Th Radiometric Age Dating Studies

In order to determine a stalagmite sample collected at cavity-E at the Karain cave during the archaeological excavation, we conducted U-Th dating on three carbonate-rich layers.[21] These layers were located at distances of 5 mm, 79 mm and 130 mm from top to bottom of the growth axis of the sample. The results of our measurements are presented in Table 3.3. The ratios in the table refer to activity ratios that are normalized to the corresponding ratios measured for the secular-equilibrium HU-1 standard. The age of YB-1 speleothem standard and HU-1 uraninite were measured simultaneously and the results were statistically not different than that of certified values.

U-Th ages obtained cannot be correlated with the ages obtained U-Th in this study and Electron Spin Resonance (ESR) techniques, which were previously applied to teeth and soil samples[19,20] collected from the Karain E-cavity.[20,21] Furthermore, the ages are too young based on a discussion made with Prof. Dr. Harun Taşkıran (oral communication, 2020) as geological layer V belongs to Lower Paleolithic stage dated back to 350 ka.

Borsato and coworkers stated that the ideal speleothem for detrital Th (clay minerals transported from surrounding land by flowing water into the cave) should have maintained a closed with no loss or gain of U and Th.[53] However, the results of U-Th age dating during this study are unreliable and require further investigations by eliminating clay from impure calcite.[54]

Table 3.3 Results of U-Th dating of stalagmite sample

Sample	**Distance from the top of the stalagmite (mm)**	**U (ppb)**	**Th (ppb)**	**(^{230}Th/ ^{232}Th)**	**(^{230}Th/^{238}U)**	**±2σ**
KR005	5	84,8	151.3	1.4	0.8	0.003
KR079	79	53.78	105.5	1.4	0.9	0.005
KR130	130	67.2	90.4	1.6	0.7	0.004
YB-1		129.3	0.59	291	0.4	0.002
HU-1		75.4	0.20	11439	1.0	0.002
Sample	**(^{234}U/ ^{238}U)**	**±2σ**	**corr. ^{230}Th Age (ka)**	**±2σ**	**corr. Initial (^{234}U/ ^{238}U)**	**±2σ**
KR005	1.11	0.001	**78**	**32**	1.27	0.123
KR079	1.13	0.002	**96**	**33**	1.36	0.186
KR130	1.13	0.002	**63**	**22**	1.24	0.067
YB-1	1.75	0.002	**30.71**	**0.15**	1.81	0.002
HU-1	1.00	0.001	**603**	**75**	1.00	0.005

CHAPTER 4

DISCUSSIONS

4.1 Climatic Controls on the Mineralogy of the Karain Cave Stalagmite

Studies on stalagmites in karstic caves, such as the Karain cave near Antalya, have shown that these carbonate deposits are important archives that can be used for past paleoclimate and paleoenvironment reconstructions. These studies require various techniques such as optical and scanning electron microscopic analysis, x-ray powder diffraction and mass spectroscopy, to reveal mineralogical, textural and morphological characteristics of the stalagmites as well as their geochemistry involving stable isotope analysis. Recording these characteristics, supported with accurate chronologies obtained by Th/U radiometric, electron spin resonance, luminescence and magnetic dating techniques provides valuable data for paleoclimate reconstructions.[11,32,34,36]

The mineralogical investigation using petrographic microscope, X-ray powder diffraction and scanning electron microscopic techniques of the stalagmite sample from the Karain cave, Antalya, revealed that the major carbonate mineral is calcite. Minor amounts of clay mineral, iron-oxide mineral, organic and a trace amount of aragonite were also identified. Calcite occurs in different shapes as coarse, columnar and equant crystals as well as half-spherulic aggregates forming thin laminae (Figure 3.2). Whitish layers formed by calcite precipitation can be observed by macroscopic and microscopic examination of the sample. However, during the growth, the continuity of these layers is interrupted by the deposition of brownish laminations composed of detrital originated iron oxide and clay minerals in some cases associated with porous texture.

One of the distinguishing characteristics of the compact calcite layers is the presence of fluid inclusions, which are small amounts of drip water that were trapped in calcite

layers during the growth of the stalagmite sample as shown in Figure 3.3.[9,10,46,55] The bottom part of the stalagmite sample consists of a lamination characteristic with half -spherulitic aggregates of calcite bone fragments and microfossils in a matrix of clay and micritic calcite.

Bar-Matthews and colleagues discussed the environmental and climatic controls of speleothem mineralogy and petrography.[32] They found that the type of carbonate mineral formed depends on factors such as the Mg/Ca ratio of the dripping water, pCO_2 levels and evaporative conditions in the cave. According to Riechelmann and coworkers, high fluid Mg/Ca ratios are typically found in dolostone host rock which leads to the precipitation of aragonite instead of calcite in dolostone caves and drip waters have high fluid Mg/Ca ratios (≥0.5), high fluid pH (>8.2) and low fluid saturation indices for calcite (<0.8).[56] These conditions are satisfied by slow drip rates, which are present under arid conditions. At high fluid Mg/Ca ratios, aragonite precipitation is kinetically stabilized and more Mg^{2+} is incorporated into the calcite crystal lattice, changing the crystal morphology.

Karain cave is situated in karstic limestone host rock and the studied stalagmite sample showed the dominance of calcite as the carbonate mineral formed during the growth of the stalagmite. This indicates that the Mg/Ca ratio was low for the precipitation of aragonite. This observation suggests that relatively humid climatic conditions during the formation of the stalagmite, although the presence of different crystal morphologies such as elongate and equant, points to slight variations in the climatic conditions.[56]

The present study suggests that a warm and wet climate dominated during the formation of the stalagmite within the geological layer V in the cave infill stratigraphy (Prof. Dr. Harun Taşkıran, oral communication). Additionally, mineralogical and petrographical observations showed that the growth layers of iron oxide (organic matter?) and clay mineral deposits alternated with calcite layers. These minerals had a detrital origin and were brought into the Karain cave either by winds or percolating waters (e.g., floods). Similarly, the formation of minor

aragonite between calcite layers defines hiatuses[10] which interrupted the continuity of the calcite deposition. This might cause small fluctuations of the paleoclimatic and paleo-environmental conditions towards drier conditions in and around the Karain cave.

4.2 Climatic Controls on the Chemistry of the Karain Cave Stalagmite

In this study, elemental composition was determined using energy dispersive x-ray analysis (EDX) while conducting micromorphological investigation through Scanning electron microscope (SEM). Moreover, $\delta^{13}C$ and $\delta^{18}O$ values were measured along the growth axis of the stalagmite sample to provide a time frame for the detectable paleoclimatological variations. Th/U dating was also performed on three points along the growth axis to determine the age of the stalagmite.

The climate and environment controls on speleothem oxygen-isotope values are widely discussed by Lachniet.[57] He emphasized that the variation of $\delta^{18}O$ values results from complicated processes in the cave system. Understanding the processes that control the fractionation of isotopes in drip water and carbonate minerals is essential for interpretating $\delta^{18}O$ values as paleoclimate and paleoenvironmental proxies.

Variations of $\delta^{13}C$ and $\delta^{18}O$ values were plotted to show their variation along the 130 mm long-growth axis of the stalagmite sample (Table 3.2 and Figure 3.5). Upward and downward fluctuations for the $\delta^{18}O$ values varied between -3.27‰ and -4.74‰ (VPDB) and $\delta^{13}C$ ranged between -2.13‰ and -5.44‰ (VPDB). Although these fluctuations took place within a narrow range, they could be divided into 5 groups along the growth axis.

At the bottom of the stalagmite sample, Group 1 and Group 3 had slightly more negative $\delta^{18}O$ and $\delta^{13}C$ values, indicating warm and wet climate conditions associated with C3 (forest) type plants. In Group 2 and Group 4, $\delta^{18}O$ values became slightly positive, meaning cooler and dryer climate associated with C4 (grassland)

type of plants. Stable isotope measurements showed no significant climatic change recorded by the stalagmite sample.

SEM-EDX analysis of the minerals (Table 3.1, Figure 3.4) revealed that calcite and clay minerals are present in the stalagmite. Chemical analysis indicated that phosphorous (P) is associated with the clay minerals forming the brown-colored lamina of the stalagmite sample. The significance of P in speleothems as a significant paleoclimate reconstruction is discussed by Frisia and coworkers.[53] Phosphorous could be derived from microbial activities in the soil and drip waters, as well as from bones in the cave environment.

Three points on the stalagmite were dated from its bottom, middle and top which measured ages of 63±22 ka, 96 ±33 ka and 78±32 ka, respectively. However, due to the presence of clay impurities in the samples, there were inconsistencies with stratigraphic observations and lower ages obtained. Martín-García explains that reverse ages are found in the recrystallized areas caused by different U-remobilization mechanisms, caused by U-leaching due to flowing waters on the surface or U-loss during the mineral transformation process. The U/Th radiometric dating analysis conducted on the samples was complicated by the presence of impurities like clay and a possible calcite to aragonite transformation mechanism. As a result, the dating results obtained from this study may have a reverse age error, similar to the one observed by Martín-García and colleagues.[11] Makhubela and colleagues also studied the age determination of calcite stalagmites in Rising Star Cave in South Africa using U-Th radioactive isotope dating.[58] They found that most of the calcite stalagmite samples had Th content between 1 ppb and 21 ppb. In comparison, the samples used in this study had much higher Th values than expected in calcite. The high Th values are attributed to the detrital clay containments with much higher (approximately 10 fold) Th content, which may have affected the dating results.

CHAPTER 5

CONCLUSIONS

The aim of this study is to analyze a stalagmite sample from the Karain Cave using a petrographic microscope, scanning electron microscope (SEM-EDX), X-ray powder diffraction (XRD), stable isotope (oxygen and carbon) and U/Th radiometric age dating techniques in order to determine, first the mineralogical, textural, micromorphological and geochemical characteristics of the stalagmite and their variation along its growth axis, secondly to interpret variations in the local microenvironment and changes of the climatic conditions in the case site by the correlation of the proxy parameters obtained from the stalagmite.

The stalagmite sample primarily comprises calcite, which forms hard and compact layers along the growth axis. Calcite has elongated and equant shapes, and in some layers, liquid inclusions are present. In addition to calcite, minor quantities of iron oxide, clay minerals and aragonite are present with the latter being identified by SEM and found associated with calcite.

These compositional characteristics of the waters are defined by the limestone host rock (rich in calcite $CaCO_3$) of the Karain cave which has a low Mg/Ca ratio. Instead of a dolostone host rock (rich in dolomite $CaMg(CO_3)_2$); The pCO_2 and evaporation conditions in the cave environment also played a role. These mineralogic and chemical conditions indicate a wet climate during the deposition of the stalagmite sample (Geological Layer V).

Thin laminae alternating with the calcite layers along the growth axis of the stalagmite, formed by clay minerals, iron oxide and a porous texture, correspond to hiatuses due to fluctuations of paleoclimatic and paleoenvironmentral conditions.

The $\delta^{13}C$ and $\delta^{18}O$ measurements from the 95 carbonate samples collected along the growth axis of the stalagmite are almost co-variant and characterized by minor

fluctuations. The $\delta^{18}O$ values vary between -3.27‰ and-4.74‰ and $\delta^{13}C$ ranges between -2.13‰ and -5.44‰. More negative $\delta^{18}O$ values, which indicate slightly warm and wet climate conditions associated with C3 (forest and grasslands) type plants are observed in Group 1. $\delta^{18}O$ values become slightly positive, indicating relatively cooler and drier climate (less rainfall amount) associated with C4 (grassland) type of plants in Group 2. Stable isotope measurements showed no significant climatic reversals recorded by the stalagmite sample.

Further studies for the paleoclimatic/paleoenvironmental investigations of the Karain Cave, Antalya it is suggested to carry out the following studies:

1. Fluid inclusion compositions can be identified to find initial drip water composition and possible paleotemperatures for paleoclimatologic research.

2. Age dating of the Karain stalagmites can be carried on by using the alternative methodology as the Electron spin resonance technique.

REFERENCES

1. Cronin, T. M. *Paleoclimates: Understanding Climate Change Past and Present*. (Columbia University Press, 2009).
2. Behrensmeyer, A. K. Climate Change and Human Evolution. *Science (1979)* **311,** 476–478 (2006).
3. Cohen, A. S., Ashley, G. M., Potts, R., Behrensmeyer, A. K., Feibel, C. & Quade, J. Paleoclimate and human evolution workshop. *Eos, Transactions American Geophysical Union* **87,** 161–161 (2006).
4. Feinberg, J. M. & Johnson, K. R. Cave and Speleothem Science: From Local to Planetary Scales. *Elements* **17,** 81–86 (2021).
5. Moore, G. V. Speleothem-A new cave term. *National Speleogical Society News* **10,** 2–2 (1952).
6. https://hbtutoring.com/understanding-geography-is-critical-to-us-understanding-the-world-around-us/.
7. Pogson, R. E., L Osborne, R. A., Colchester, D. M. & and, R. *Minerals of Jenolan Caves, New South Wales, Australia: Geological and Biological Interactions*. (2014). at <http://escholarship.library.usyd.edu.au/journals/index.php/LINJenolan.Theirchemicalgroupsincludecarbonates:>
8. Fairchild, I. J. & A. Baker. *Speleothem Science: From Process to Past Environments*. (Wiley-Blackwell, 2012).
9. McDermott Frank, Schwarcz, H. & Rowe Peter J. in *Isotopes in Palaeoenvironmental Research* (ed. Leng, M. J.) 185–225 (Springer Netherlands, 2006).

10. Polyak, V. J., Asmerom, Y., Lachniet, M. S. & Provencio, P. P. High-resolution examination of drought and pullivial events in southern USA stalagmites. in *Proceedings of the 17th International Congress of Speleology* 241–244 (2017).

11. Martín-García, R., Alonso-Zarza, A. M., Frisia, S., Rodríguez-Berriguete, Á., Drysdale, R. & Hellstrom, J. Effect of aragonite to calcite transformation on the geochemistry and dating accuracy of speleothems. An example from Castañar Cave, Spain. *Sediment Geol* **383,** 41–54 (2019).

12. Elias, S. Reference Module in Earth Systems and Environmental Sciences. (2013).

13. Kökten, İ. K. Bazı prehistorik istasyonlar hakkında yeni gözlemler. *Dil ve Tarih Coğrafya Dergisi* **2,** 223–236 (1947).

14. Yalçınkaya, I. 1991 Karain Kazıları. in *XIII. Kazı Sonuçları Toplantısı* 33–54 (1991).

15. Yalçınkaya, I., Taşkıran, H., Özçelik, K. & Kösem, M. B. 2009 Yılı Karain Mağarası Kazıları. in *32. Kazı Sonuçları Toplantısı, 3. Cilt,* 22–35 (2011).

16. Taşkıran, H. Türkiye Paleolitik kronolojisi. *Anadolu Prehistorya araştırmaları Dergisi (APAD)* **1,** 113–121 (2015).

17. Koşun, E., Varol, B. & Taşkıran, H. . in *Landscapes and Landforms of Turkey, World Geomorphological Landscape Series* (eds. C. Kuzucuoğlu, A.Çiner & N.Kazancı) 207–217 (Springer, 2019).

18. Yaman, İ. D. Orta Paleolitik Dönem'de Sedimantoloji ve Yontmataş Analizleri Işığında Karain Mağarası E ve B Gözleri Bağlantısı. (2013).

19. Djerrab, A. & Aïfa, T. Contribution of rock magnetism to stratigraphy and palaeoenvironment of the Karaïn cave infill, Antalya, Turkey. *Studia Geophysica et Geodaetica* **54,** 49–76 (2010).

20. Rink, W. I., Schwarcz, H. P., Grün, R., Yalçinkaya, I., Taskiran, H., Otte, M., Valladas, H., Mercier, N., Bar-Yosef, O. & Kozlowski, J. ESR Dating of the Last Interglacial Mousterian at Karaïn Cave, Southern Turkey. *J Archaeol Sci* **21,** 839–849 (1994).

21. Yalçınkaya, I., Otte, M., Taşkıran, H., Kösem, B. & Ceylan, K. 1985-1995 Karain kazıları ışığında Anadolu Paleolitiğinin önemi. in *XVIII. Kazı Sonuçları Toplantısı,1.Cilt* 1–9 (1995).

22. McDermott, F. Palaeo-climate reconstruction from stable isotope variations in speleothems: a review. *Quat Sci Rev* **23,** 901–918 (2004).

23. Spötl, C. & Boch, R. in *Encyclopedia of Caves* (ed. William B. White David C. Culver) 838–844 (Elsevier, 2012). doi:10.1016/B978-0-12-814124-3.00128-X

24. Engin, B., Aydaş, C., Özkul, M., Zeyrek, C. T., Büyüm, M. & Gül, A. ESR dating of stalagmite from Keloğlan cave in the southwestern part of Turkey. *Radiation Effects and Defects in Solids* **165,** 944–957 (2010).

25. Watanabe, S., Cano, N. F., Rao, T. K. G., Silva-Carrera, B. N., Carmo, L. S., Quina, A. J. A., Gennari, R. F., Munita, C. S., Ayala-Arenas, J. S. & Fernandes, B. G. Dating stalagmite from Caverna do Diabo (Devil´S Cave) by TL and EPR techniques. *An Acad Bras Cienc* **88,** 2137–2142 (2016).

26. Yalçınkaya, I. 1985 yılı Karain kazıları. in *VII.Kazı Sonuçları Toplantısı, 1. Cilt* 21–29 (1987).

27. Kuzucuoğlu, C., Çiner, A. & Kazancı, N. in *Landscapes and Landforms of Turkey, World Geomorphological Landscape Series* (eds. Kuzucuoğlu, C., A.Çiner & N.Kazancı) 41–187 (Springer, 2019).

28. Pawlikowski, M. ,. Karain and Öküzini Caves, Turkey. General Geology of Area. Preliminary Report. *Türkiye Coğrafyası Araştırma ve Uygulama Merkezi Dergisi* **3,** 351–369 (1995).

29. Pickering, J. L., Goodbred, S. L., Beam, J. C., Ayers, J. C., Covey, A. K., Rajapara, H. M. & Singhvi, A. K. Terrace formation in the upper Bengal basin since the Middle Pleistocene: Brahmaputra fan delta construction during multiple highstands. *Basin Research* **30,** 550–567 (2018).

30. Yalçınkaya, I., Taşkıran, H., Kartal, M., Kösem, M. B., Ceylan, K., Erek, C. M. , Atıcı, A. L. & Otte, M. 1995 ve 1996 Yılları Karain Kazıları. in *XIX. Kazı Sonuçları Toplantısı,1.Cilt* 17–45 (1998).

31. Taşkıran, H. in *Anatolian Metal VII* (ed. Yalçın Ünsal) 43–51 (2016).

32. Bar-Matthews, M., Matthews, A. & Ayalon, A. Environmental Controls of Speleothem Mineralogy in a Karstic Dolomitic Terrain (Soreq Cave, Israel). *J Geol* **99,** 189–207 (1991).

33. Self, C. A. & Hill, C. A. How Speleothems Grow: An Introduction to the Ontogeny of Cave Minerals. *Journal of Cave and Karst Studies* **65,** 130–151 (2003).

34. White, W. Cave sediments and paleoclimate. *Journal of Cave and Karst Studies* **69,** 76–93 (2007).

35. Erkan, G. Konya Kapalı Havzası (Orta Anadolu) Geç Pleyistosen-Holosen İkliminin Dikit Kayıtları İle Kurgulanması. (2012).

36. Duan, W., Kotlia, B. S. & Tan, M. Mineral composition and structure of the stalagmite laminae from Chulerasim cave, Indian Himalaya, and the significance for palaeoclimatic reconstruction. *Quaternary International* **298,** 93–97 (2013).

37. Özbek, O., Erdoğu, B., Uysal, I. T. & Ulusoy, Ü. Speleothems of Catalhoyuk, Turkey. *Mediterranean Archaeology and Archaeometry* **13,** 21–30 (2013).

38. Perrin, C., Prestimonaco, L., Servelle, G., Tilhac, R., Maury, M. & Cabrol, P. Aragonite-Calcite Speleothems: Identifying Original and Diagenetic Features. *Journal of Sedimentary Research* **84,** 245–269 (2014).

39. Shen, X., Wan, S., Colin, C., Tada, R., Shi, X., Pei, W., Tan, Y., Jiang, X. & Li, A. Increased seasonality and aridity drove the C4 plant expansion in Central Asia since the Miocene–Pliocene boundary. *Earth Planet Sci Lett* **502,** 74–83 (2018).

40. Baldini, J. U. L. The geochemistry of cave calcite deposits as a record of past climate. *The Sedimentary Record* **8,** 4–9 (2010).

41. Zhu, X., Zhang, M., Lin, Y., Qin, J. & Yang, Y. Carbon isotopic records from stalagmites and the signification of paleo-ecological environment in the area of Guangxi—Guizhou, China. *Environmental Geology* **51,** 267–273 (2006).

42. Aydın, Y. Pleistosen Dönem'den Bir Alt Paleolitik Kesit: Karain. *Türkiye Jeoloji Bülteni / Geological Bulletin of Turkey* 29–68 (2017). doi:10.25288/tjb.360607

43. Yalçınkaya, I., Taşkıran, H., Kartal, M., Özçelik, K. & Sevencan, B. C. 2003 Yılı Karain Mağarası Kazısı. in *26. Kazı Sonuçları Toplantısı, 2. Cilt* 215–224 (2005).

44. Yalçınkaya, I., Taşkıran, H., Kartal, M., Özçelik, K. & Kösem, M. B. 2004 Yılı Karain Mağarası Kazıları. in *27. Kazı Sonuçları Toplantısı, 1. Cilt,* 403–418 (2006).

45. Yalçınkaya, I., Taşkıran, H., Kartal, M., Özçelik, K., Kösem, M. B. & Kartal, G. 2005 Yılı Karain Mağarası Kazıları. in *28. Kazı Sonuçları Toplantısı, 1. Cilt* 539–558 (2007).

46. Yalçınkaya, I., Taşkıran, H., Kartal, M., Özçelik, K., Kösem, M. B. & Kartal, G. 2008 Yılı Karain Mağarası Kazıları. in *31. Kazı Sonuçları Toplantısı, 4. Cilt* 41–62 (2010).

47. Yalçınkaya, I. 1989 Yılı Karain Kazıları. in *XII. Kazı Sonuçları Toplantısı, 1. Cilt* 43–70 (1991).

48. Gribble, C. D. & Hall, A. J. *Optical Mineralogy, Principles and Practice*. (UCL Press, 1997).

49. R. Gonfiantini, W. Stichler & K. Rozanski. Reference and intercomparison materials for stable isotopes of light elements. in *Standards and Intercomparison Materials Distributed by the International Atomic Energy Agency for Stable Isotope Measurements - Reference and intercomparison materials for stable isotopes of light elements* 13–29 (1993).

50. Chen, P.-Y. Table Of Key Lines in X-Ray Powder Diffraction Patterns of Minerals in Clays and Associated Rocks. *Geological Survey Occasional Paper 21* 1–67 (1971).

51. Moore, D. M. & Reynolds, Jr. , R. C. *X-Ray Diffraction And The Identification and Analysis of Clay Minerals*. (Oxford University Press, 1997).

52. Zhang, R., Schwarcz, H. P., Ford, D. C. & Beddows, P. A. SEM and petrographic studies of stalagmite caps and trapping of fluid inclusions. in (2005).

53. Frisia, S., Borsato, A., Drysdale, R. N., Paul, B., Greig, A. & Cotte, M. A re-evaluation of the palaeoclimatic significance of phosphorus variability in speleothems revealed by high-resolution synchrotron micro XRF mapping. *Climate of the Past* **8,** 2039–2051 (2012).

54. Farkh, S., Harb, N., Haddad, K., Zeaiter, Z. & Farkh, S. Improvement Of The U-Th Method For Dating Of Impure Calcite Having A Large Amount

Of Clay And Very Low Uranium Content. *International Journal of Scientific & Technology Research* **4,** 334–336 (2015).

55. Affolter, S., Fleitmann, D. & Leuenberger, M. New online method for water isotope analysis of speleothem fluid inclusions using laser absorption spectroscopy (WS-CRDS). *Climate of the Past* **10,** 1291–1304 (2014).

56. Riechelmann, S., Schröder-Ritzrau, A., Wassenburg, J. A., Schreuer, J., Richter, D. K., Riechelmann, D. F. C., Terente, M., Constantin, S., Mangini, A. & Immenhauser, A. Physicochemical characteristics of drip waters: Influence on mineralogy and crystal morphology of recent cave carbonate precipitates. *Geochim Cosmochim Acta* **145,** 13–29 (2014).

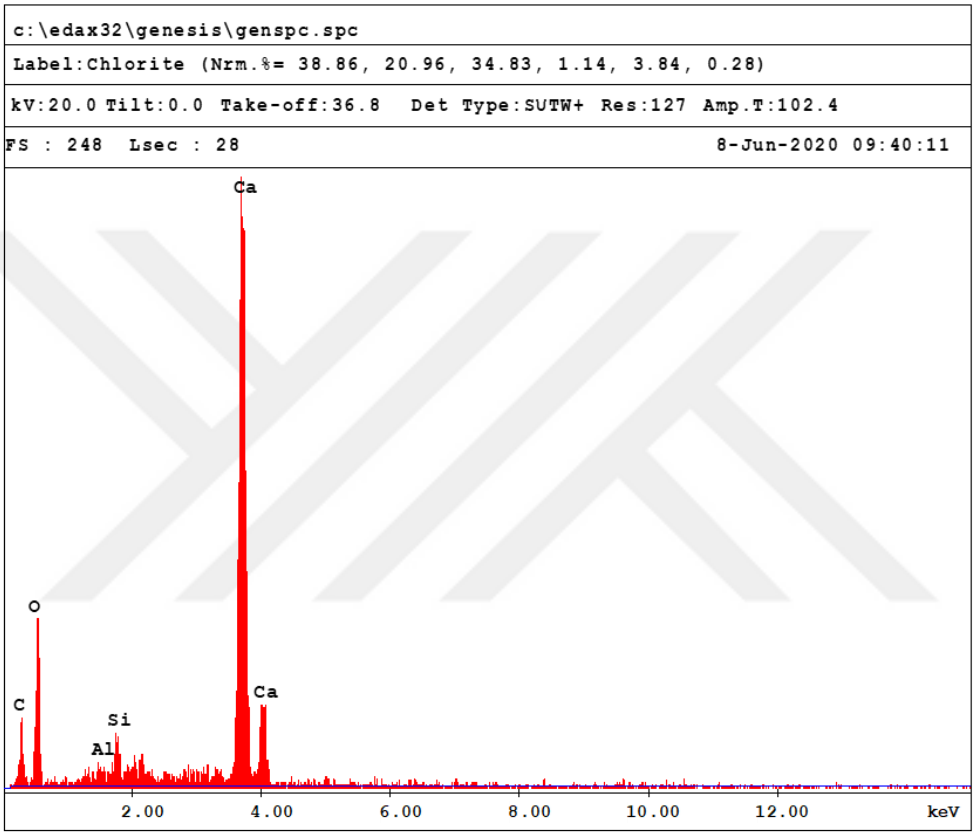
57. Lachniet, M. S. Climatic and environmental controls on speleothem oxygen-isotope values. *Quat Sci Rev* **28,** 412–432 (2009).

58. Makhubela, T. V. & Kramers, J. D. Testing a new combined (U,Th)–He and U/Th dating approach on Plio-Pleistocene calcite speleothems. *Quat Geochronol* **67,** 101234 (2022).

APPENDICES

A. SEM-EDX Analysis of Stalagmite Samples

Sample No: 1-3



EDAX ZAF Quantification (Standardless)
Element Normalized
SEC Table : Default

Element	Wt %	At %	K-Ratio	Z	A	F
C K	13.20	23.28	0.0513	1.0463	0.3715	1.0010
O K	37.87	50.15	0.0508	1.0286	0.1304	1.0001
AlK	1.07	0.84	0.0063	0.9577	0.6130	1.0044
SiK	1.91	1.44	0.0139	0.9856	0.7315	1.0074
CaK	45.95	24.29	0.4423	0.9579	1.0049	1.0000
Total	100.00	100.00				

Element	Net Inte.	Bkgd Inte.	Inte. Error	P/B
C K	3.99	0.21	9.80	19.17
O K	10.31	0.21	5.92	49.50
AlK	1.80	0.28	15.86	6.50
SiK	3.71	0.31	10.45	11.89
CaK	73.47	0.38	2.18	192.45

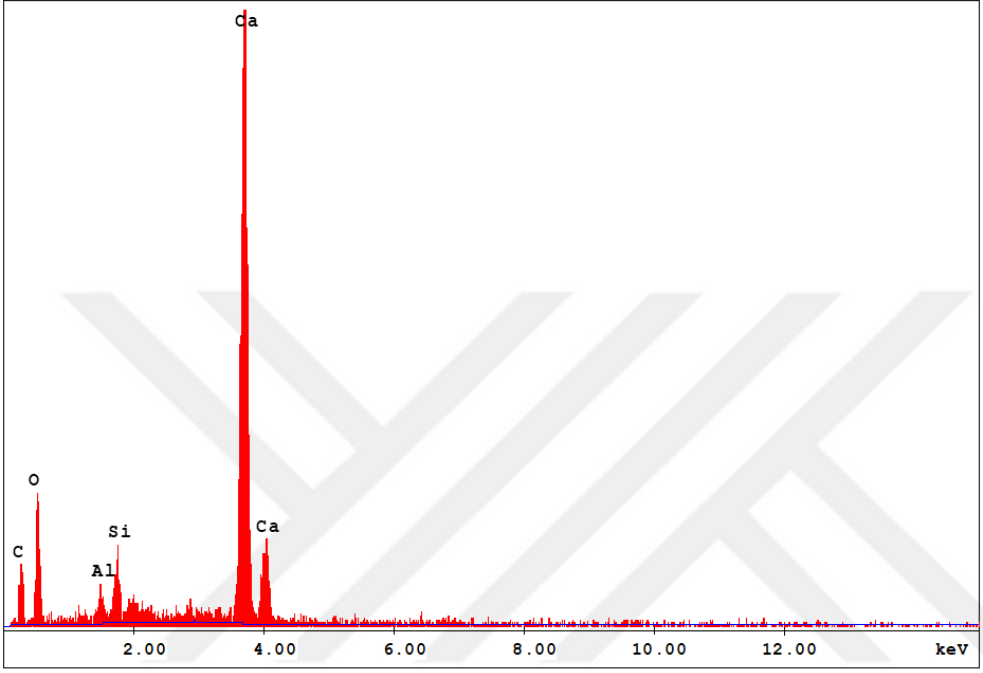
Sample No: 1-4

c:\edax32\genesis\genspc.spc

Label:Chlorite (Nrm.%= 38.86, 20.96, 34.83, 1.14, 3.84, 0.28)

kV:20.0 Tilt:0.0 Take-off:36.8 Det Type:SUTW+ Res:127 Amp.T:102.4

FS : 286 Lsec : 36 8-Jun-2020 09:42:42



EDAX ZAF Quantification (Standardless)
Element Normalized
SEC Table : Default

Element	Wt %	At %	K-Ratio	Z	A	F
C K	13.28	23.83	0.0483	1.0479	0.3464	1.0010
O K	35.07	47.24	0.0460	1.0302	0.1273	1.0001
AlK	1.65	1.32	0.0098	0.9591	0.6178	1.0049
SiK	3.14	2.41	0.0228	0.9871	0.7300	1.0074
CaK	46.86	25.20	0.4501	0.9595	1.0012	1.0000
Total	100.00	100.00				

Element	Net Inte.	Bkgd Inte.	Inte. Error	P/B
C K	3.38	0.16	9.36	20.83
O K	8.42	0.16	5.78	51.83
AlK	2.54	0.24	11.26	10.44
SiK	5.49	0.49	7.62	11.28
CaK	67.44	0.38	2.01	178.00

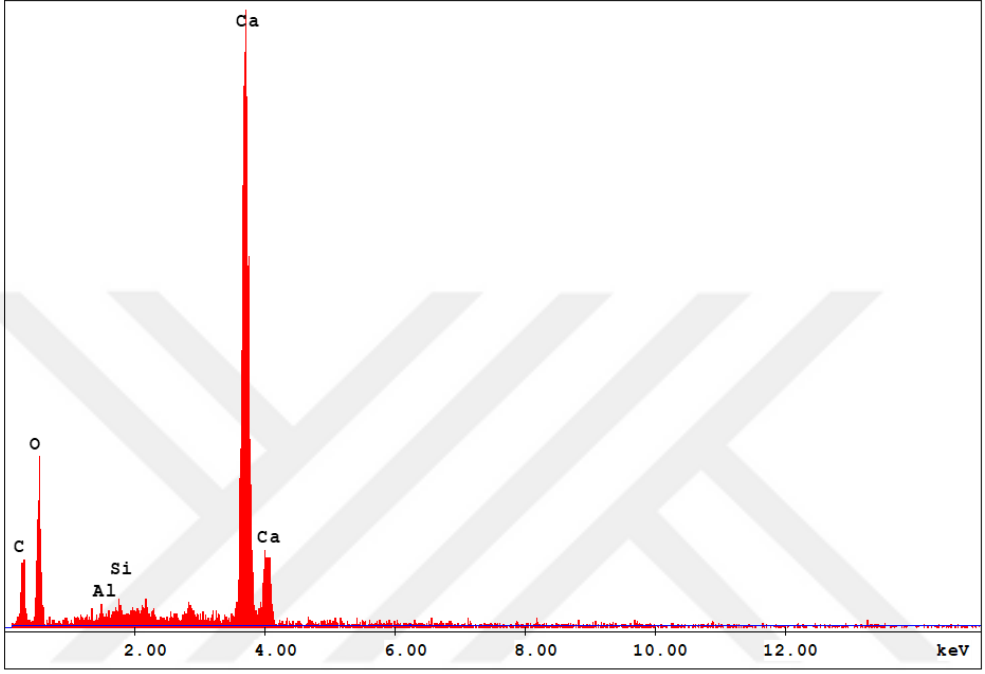
Sample No: 1-5

c:\edax32\genesis\genspc.spc

Label:Chlorite (Nrm.%= 38.86, 20.96, 34.83, 1.14, 3.84, 0.28)

kV:20.0 Tilt:0.0 Take-off:36.8 Det Type:SUTW+ Res:127 Amp.T:102.4

FS : 390 Lsec : 39 8-Jun-2020 09:44:35



EDAX ZAF Quantification (Standardless)
Element Normalized
SEC Table : Default

Element	Wt %	At %	K-Ratio	Z	A	F
C K	14.45	25.25	0.0590	1.0456	0.3900	1.0010
O K	37.40	49.07	0.0497	1.0280	0.1293	1.0001
AlK	0.79	0.61	0.0046	0.9571	0.6130	1.0042
SiK	1.21	0.91	0.0088	0.9850	0.7343	1.0076
CaK	46.15	24.17	0.4450	0.9573	1.0073	1.0000
Total	100.00	100.00				

Element	Net Inte.	Bkgd Inte.	Inte. Error	P/B
C K	5.01	0.15	7.28	33.33
O K	11.02	0.15	4.83	73.33
AlK	1.45	0.20	14.83	7.25
SiK	2.58	0.23	10.68	11.44
CaK	80.77	0.28	1.77	293.18

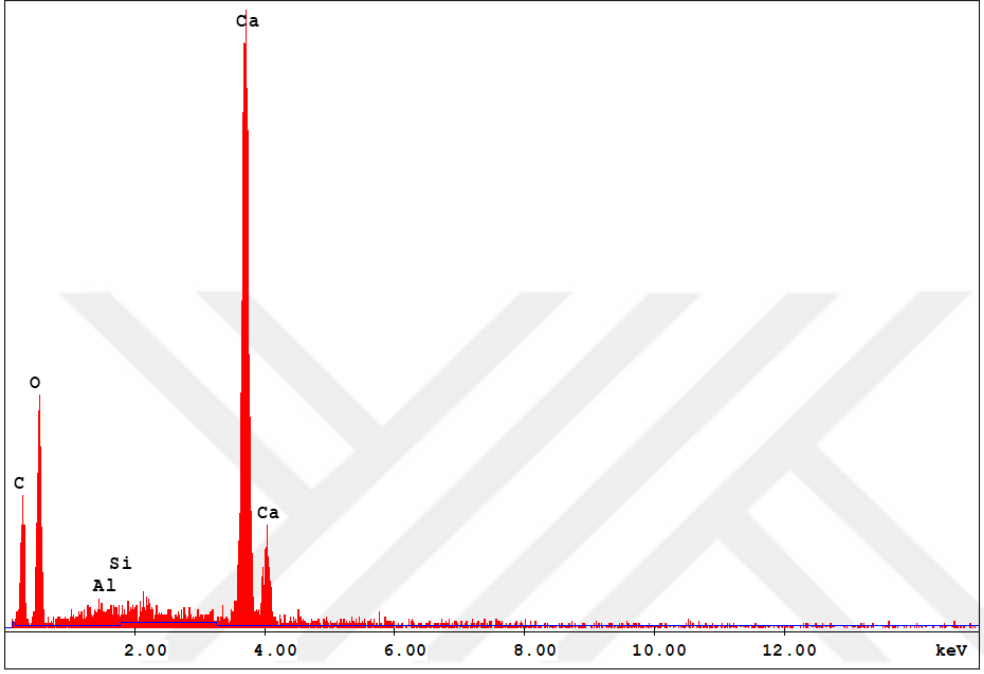
Sample No: 1-6

c:\edax32\genesis\genspc.spc

Label:Chlorite (Nrm.%= 38.86, 20.96, 34.83, 1.14, 3.84, 0.28)

kV:20.0 Tilt:0.0 Take-off:36.8 Det Type:SUTW+ Res:127 Amp.T:102.4

FS : 276 Lsec : 23 8-Jun-2020 09:47:01



EDAX ZAF Quantification (Standardless)
Element Normalized
SEC Table : Default

Element	Wt %	At %	K-Ratio	Z	A	F
C K	19.35	30.89	0.0837	1.0383	0.4165	1.0008
O K	41.98	50.32	0.0620	1.0208	0.1446	1.0001
AlK	0.75	0.53	0.0045	0.9506	0.6238	1.0034
SiK	0.55	0.38	0.0040	0.9783	0.7445	1.0064
CaK	37.38	17.88	0.3592	0.9500	1.0115	1.0000
Total	100.00	100.00				

Element	Net Inte.	Bkgd Inte.	Inte. Error	P/B
C K	10.87	0.25	6.34	43.33
O K	20.98	0.25	4.52	83.67
AlK	2.13	0.33	16.05	6.37
SiK	1.80	0.42	18.46	4.30
CaK	99.60	0.46	2.06	216.64

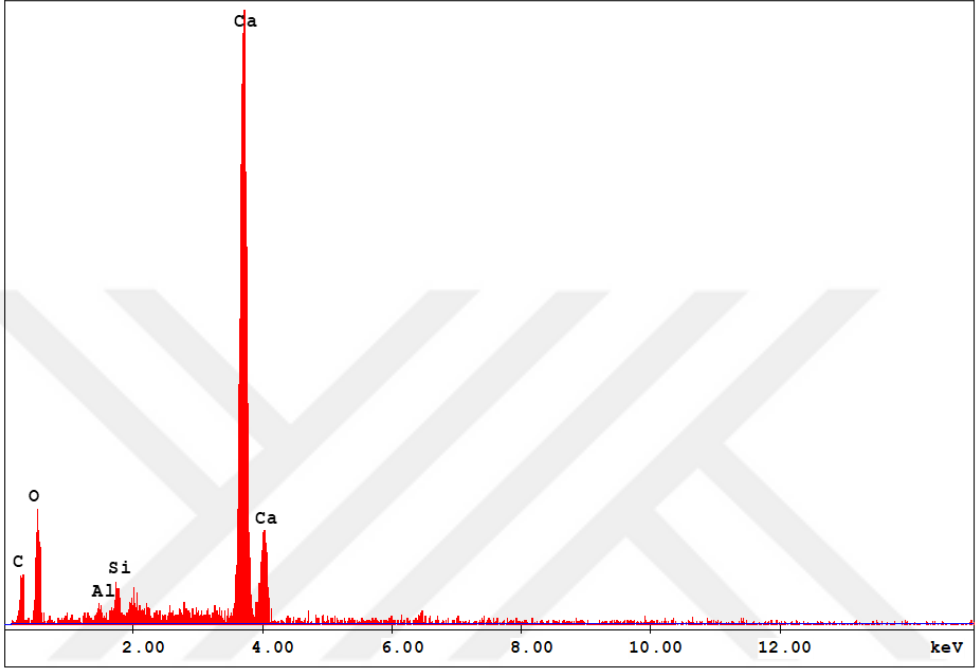
Sample No: 1-7

c:\edax32\genesis\genspc.spc

Label:Chlorite (Nrm.%= 38.86, 20.96, 34.83, 1.14, 3.84, 0.28)

kV:20.0 Tilt:0.0 Take-off:36.4 Det Type:SUTW+ Res:127 Amp.T:102.4

FS : 338 Lsec : 54 8-Jun-2020 09:49:09



EDAX ZAF Quantification (Standardless)
Element Normalized
SEC Table : Default

Element	Wt %	At %	K-Ratio	Z	A	F
C K	12.08	22.39	0.0468	1.0503	0.3688	1.0011
O K	33.52	46.66	0.0416	1.0326	0.1203	1.0001
AlK	0.94	0.78	0.0055	0.9613	0.6073	1.0048
SiK	1.97	1.56	0.0143	0.9892	0.7276	1.0082
CaK	51.49	28.61	0.4973	0.9619	1.0040	1.0000
Total	100.00	100.00				

Element	Net Inte.	Bkgd Inte.	Inte. Error	P/B
C K	2.33	0.11	9.32	21.00
O K	5.42	0.11	5.96	48.83
AlK	1.02	0.15	15.32	6.87
SiK	2.46	0.17	9.24	14.78
CaK	53.24	0.20	1.87	261.55

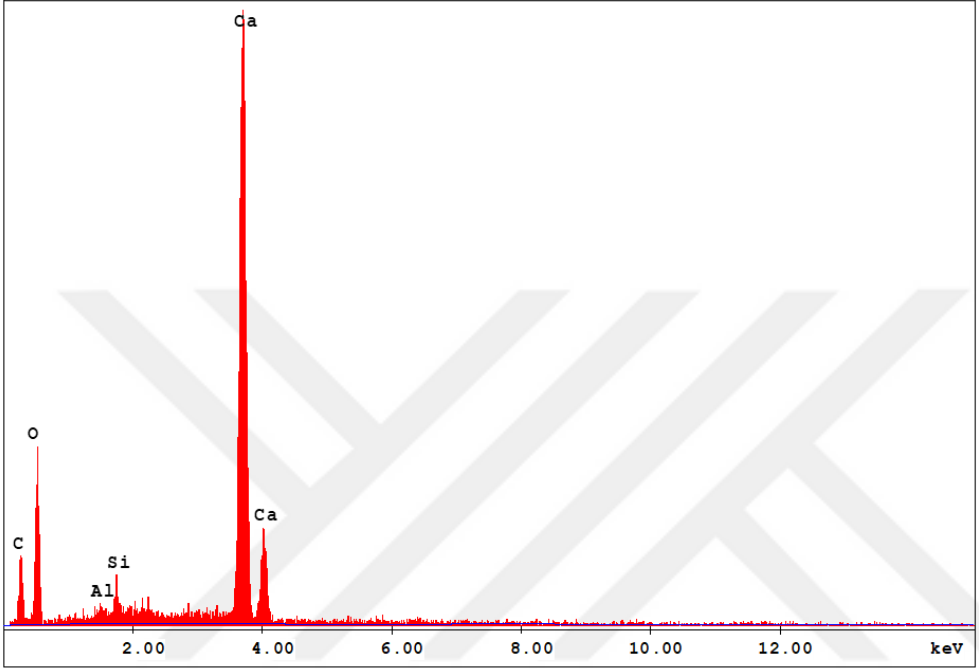
Sample No: 1-9

c:\edax32\genesis\genspc.spc

Label:Chlorite (Nrm.%= 38.86, 20.96, 34.83, 1.14, 3.84, 0.28)

kV:20.0 Tilt:0.0 Take-off:37.2 Det Type:SUTW+ Res:127 Amp.T:102.4

FS : 526 Lsec : 72 8-Jun-2020 09:56:06

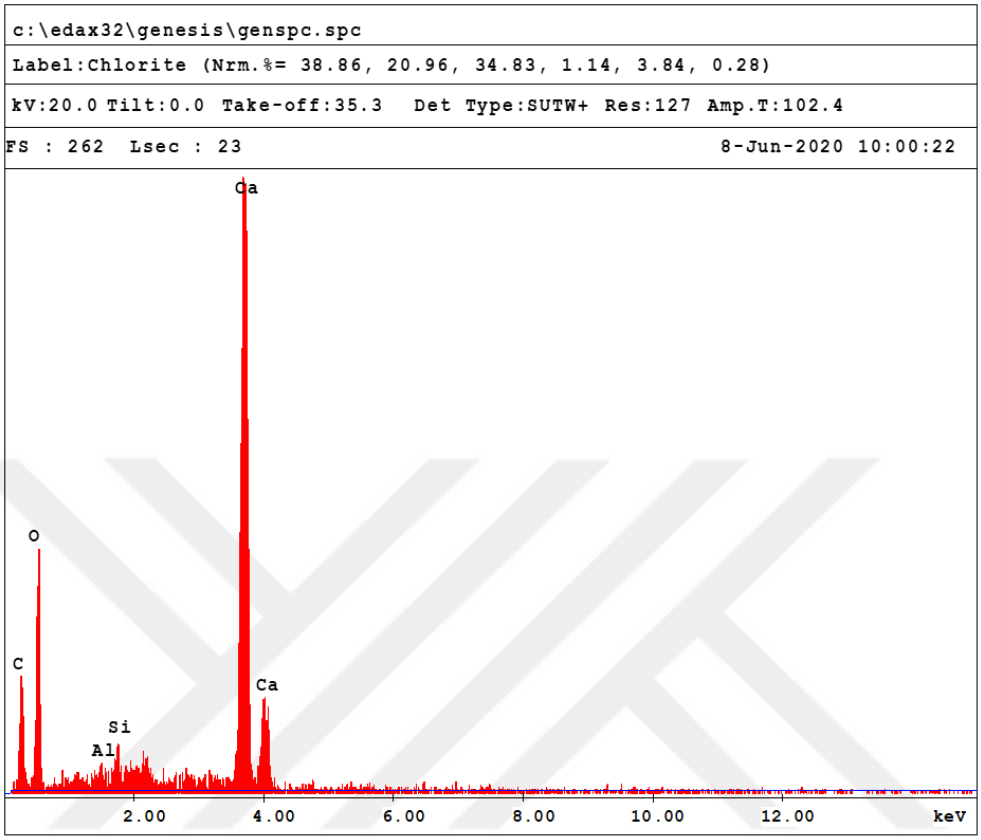


EDAX ZAF Quantification (Standardless)
Element Normalized
SEC Table : Default

Element	Wt %	At %	K-Ratio	Z	A	F
C K	14.65	25.48	0.0584	1.0452	0.3808	1.0010
O K	37.51	48.97	0.0506	1.0276	0.1313	1.0001
AlK	0.89	0.69	0.0053	0.9568	0.6181	1.0044
SiK	1.75	1.30	0.0128	0.9846	0.7375	1.0074
CaK	45.21	23.56	0.4352	0.9569	1.0060	1.0000
Total	100.00	100.00				

Element	Net Inte.	Bkgd Inte.	Inte. Error	P/B
C K	4.02	0.08	5.96	48.83
O K	9.07	0.08	3.92	110.17
AlK	1.33	0.22	11.71	6.06
SiK	3.00	0.25	7.29	12.17
CaK	63.51	0.30	1.48	210.41

Sample No: 2-2



EDAX ZAF Quantification (Standardless)
Element Normalized
SEC Table : Default

Element	Wt %	At %	K-Ratio	Z	A	F
C K	19.38	31.17	0.0776	1.0390	0.3853	1.0008
O K	40.48	48.88	0.0584	1.0215	0.1411	1.0001
AlK	0.99	0.71	0.0058	0.9512	0.6196	1.0038
SiK	1.85	1.27	0.0135	0.9790	0.7389	1.0062
CaK	37.30	17.98	0.3577	0.9507	1.0086	1.0000
Total	100.00	100.00				

Element	Net Inte.	Bkgd Inte.	Inte. Error	P/B
C K	10.23	0.26	6.67	39.33
O K	20.29	0.26	4.68	78.00
AlK	2.90	0.35	13.60	8.37
SiK	6.24	0.39	8.84	16.00
CaK	103.55	0.48	2.06	217.18

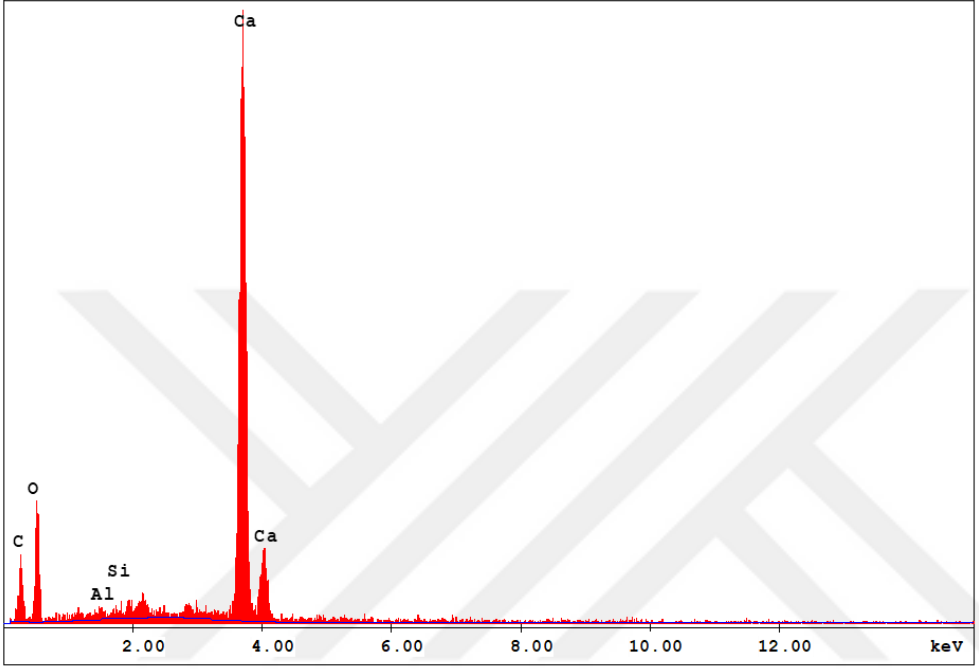
Sample No: 2-3

c:\edax32\genesis\genspc.spc

Label:Chlorite (Nrm.%= 38.86, 20.96, 34.83, 1.14, 3.84, 0.28)

kV:20.0 Tilt:0.0 Take-off:35.3 Det Type:SUTW+ Res:127 Amp.T:102.4

FS : 495 Lsec : 43 8-Jun-2020 10:03:24



EDAX ZAF Quantification (Standardless)
Element Normalized
SEC Table : Default

Element	Wt %	At %	K-Ratio	Z	A	F
C K	14.53	25.72	0.0615	1.0467	0.4040	1.0010
O K	35.94	47.75	0.0455	1.0291	0.1231	1.0001
AlK	0.60	0.47	0.0035	0.9581	0.6018	1.0041
SiK	0.44	0.33	0.0032	0.9860	0.7266	1.0079
CaK	48.49	25.72	0.4690	0.9584	1.0093	1.0000
Total	100.00	100.00				

Element	Net Inte.	Bkgd Inte.	Inte. Error	P/B
C K	5.76	0.28	6.65	20.67
O K	11.25	0.14	4.60	80.67
AlK	1.23	0.60	19.33	2.04
SiK	1.05	0.84	24.04	1.25
CaK	96.47	0.58	1.56	166.04

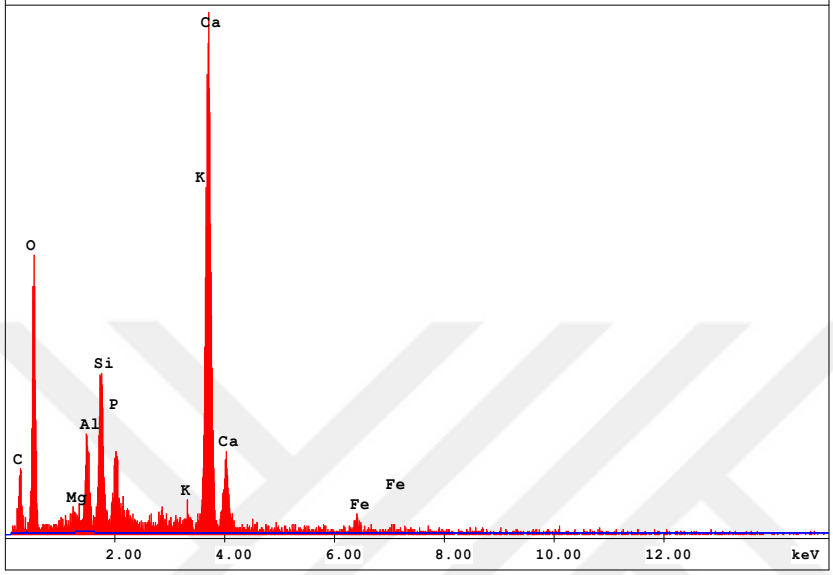
Sample No: 2-6

c:\edax32\genesis\genspc.spc

Label:Chlorite (Nrm.%= 38.86, 20.96, 34.83, 1.14, 3.84, 0.28)

kV:20.0 Tilt:0.0 Take-off:35.8 Det Type:SUTW+ Res:127 Amp.T:102.4

FS : 301 Lsec : 29 8-Jun-2020 10:13:34



EDAX ZAF Quantification (Standardless)
Element Normalized
SEC Table : Default

Element	Wt %	At %	K-Ratio	Z	A	F
C K	15.51	25.72	0.0402	1.0441	0.2484	1.0006
O K	39.58	49.28	0.0661	1.0265	0.1626	1.0002
MgK	0.92	0.76	0.0044	0.9848	0.4865	1.0035
AlK	3.54	2.61	0.0213	0.9558	0.6269	1.0053
SiK	6.41	4.55	0.0456	0.9837	0.7191	1.0056
P K	3.20	2.06	0.0232	0.9483	0.7612	1.0073
K K	0.92	0.47	0.0087	0.9334	0.9613	1.0605
CaK	27.68	13.76	0.2588	0.9554	0.9776	1.0011
FeK	2.25	0.80	0.0191	0.8682	0.9797	1.0000
Total	100.00	100.00				

Element	Net Inte.	Bkgd Inte.	Inte. Error	P/B
C K	5.96	0.20	7.81	29.17
O K	25.73	0.20	3.67	125.83
MgK	2.49	0.37	13.35	6.64
AlK	11.83	0.55	5.61	21.69
SiK	23.62	0.31	3.85	77.00
P K	10.91	0.31	5.75	35.56
K K	3.10	0.34	11.58	9.10
CaK	83.48	0.37	2.03	222.64
FeK	2.83	0.48	12.69	5.93

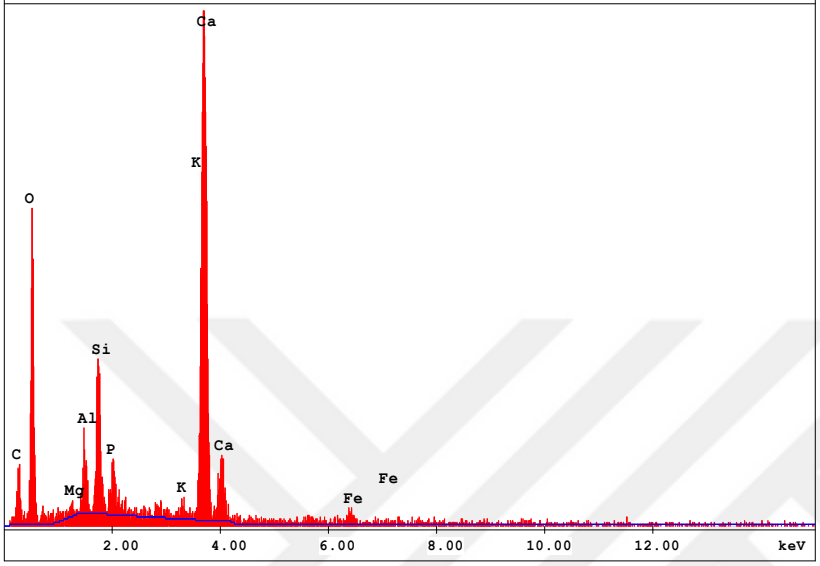
Sample No: 2-9

c:\edax32\genesis\genspc.spc

Label:Chlorite (Nrm.%= 38.86, 20.96, 34.83, 1.14, 3.84, 0.28)

kV:20.0 Tilt:0.0 Take-off:36.9 Det Type:SUTW+ Res:127 Amp.T:102.4

FS : 284 Lsec : 46 8-Jun-2020 10:24:34



EDAX ZAF Quantification (Standardless)
Element Normalized
SEC Table : Default

Element	Wt %	At %	K-Ratio	Z	A	F
C K	13.13	22.03	0.0369	1.0439	0.2694	1.0007
O K	42.53	53.57	0.0712	1.0264	0.1632	1.0002
MgK	0.54	0.45	0.0026	0.9847	0.4795	1.0031
AlK	2.51	1.88	0.0150	0.9557	0.6235	1.0051
SiK	6.07	4.35	0.0436	0.9836	0.7263	1.0056
P K	2.05	1.34	0.0151	0.9483	0.7709	1.0082
K K	0.55	0.28	0.0053	0.9334	0.9686	1.0709
CaK	30.51	15.34	0.2873	0.9554	0.9847	1.0011
FeK	2.11	0.76	0.0179	0.8682	0.9782	1.0000
Total	100.00	100.00				

Element	Net Inte.	Bkgd Inte.	Inte. Error	P/B
C K	3.20	0.13	8.49	25.00
O K	16.07	0.13	3.67	125.67
MgK	0.83	0.92	28.67	0.91
AlK	4.79	1.19	8.16	4.02
SiK	12.93	1.34	4.46	9.63
P K	4.07	1.15	9.05	3.54
K K	1.09	0.85	22.44	1.27
CaK	52.97	0.70	2.03	75.33
FeK	1.51	0.30	14.01	5.07

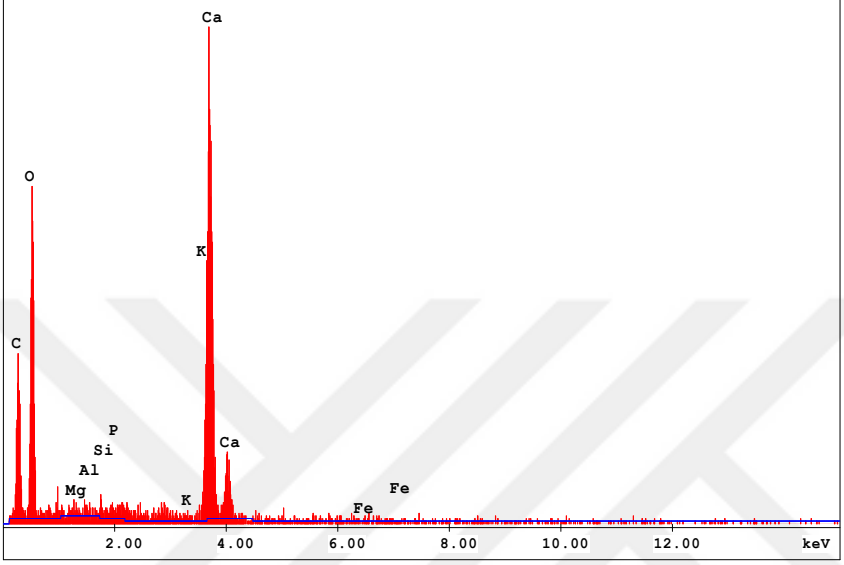
Sample No: 2-10

c:\edax32\genesis\genspc.spc

Label:Chlorite (Nrm.%= 38.86, 20.96, 34.83, 1.14, 3.84, 0.28)

kV:20.0 Tilt:0.0 Take-off:36.9 Det Type:SUTW+ Res:127 Amp.T:102.4

FS : 200 Lsec : 15 8-Jun-2020 10:27:55



EDAX ZAF Quantification (Standardless)
Element Normalized
SEC Table : Default

Element	Wt %	At %	K-Ratio	Z	A	F
C K	24.38	35.29	0.1072	1.0298	0.4269	1.0007
O K	48.39	52.60	0.0851	1.0125	0.1738	1.0000
MgK	0.29	0.21	0.0014	0.9716	0.4888	1.0013
AlK	0.39	0.25	0.0023	0.9431	0.6366	1.0025
SiK	0.38	0.24	0.0028	0.9706	0.7596	1.0048
P K	0.43	0.24	0.0035	0.9341	0.8510	1.0088
K K	0.29	0.13	0.0029	0.9197	1.0039	1.0826
CaK	25.45	11.04	0.2426	0.9415	1.0127	1.0000
FeK	0.00	0.00	0.0000	0.8550	0.9896	1.0000
Total	100.00	100.00				

Element	Net Inte.	Bkgd Inte.	Inte. Error	P/B
C K	18.34	0.76	6.13	24.00
O K	37.95	0.76	4.18	49.67
MgK	0.89	1.53	56.24	0.58
AlK	1.46	1.53	36.64	0.96
SiK	1.66	1.34	31.72	1.24
P K	1.85	1.15	27.80	1.61
K K	1.15	0.64	34.25	1.80
CaK	88.37	1.34	2.72	66.10
FeK	0.00	0.89	0.00	0.00

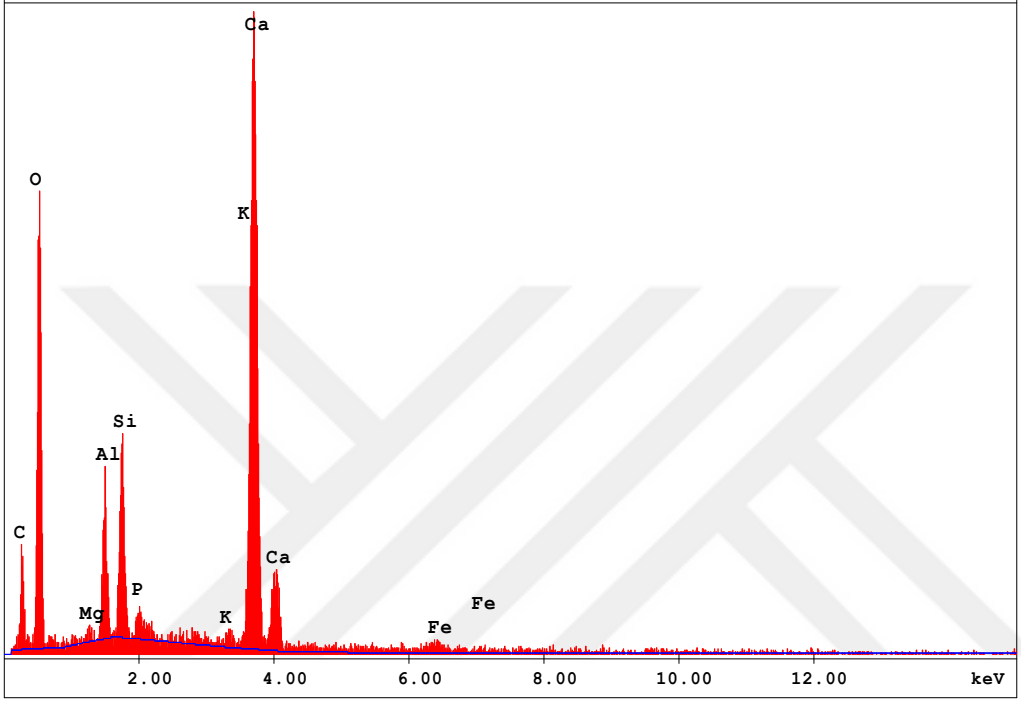
Sample No: 2-11

c:\edax32\genesis\genspc.spc

Label:Chlorite (Nrm.%= 38.86, 20.96, 34.83, 1.14, 3.84, 0.28)

kV:20.0 Tilt:0.0 Take-off:36.9 Det Type:SUTW+ Res:127 Amp.T:102.4

FS : 486 Lsec : 68 8-Jun-2020 10:28:45



EDAX ZAF Quantification (Standardless)
Element Normalized
SEC Table : Default

Element	Wt %	At %	K-Ratio	Z	A	F
C K	14.35	23.09	0.0428	1.0401	0.2868	1.0007
O K	46.31	55.96	0.0830	1.0226	0.1754	1.0001
MgK	0.40	0.32	0.0019	0.9811	0.4832	1.0030
AlK	3.71	2.66	0.0223	0.9523	0.6289	1.0043
SiK	5.18	3.56	0.0367	0.9800	0.7198	1.0046
P K	0.82	0.51	0.0060	0.9443	0.7737	1.0075
K K	0.55	0.27	0.0053	0.9295	0.9745	1.0662
CaK	27.13	13.09	0.2556	0.9515	0.9893	1.0008
FeK	1.56	0.54	0.0133	0.8645	0.9831	1.0000
Total	100.00	100.00				

TEZ İZİN FORMU / THESIS PERMISSION FORM

ENSTİTÜ / INSTITUTE

Fen Bilimleri Enstitüsü / Graduate School of Natural and Applied Sciences	x
Sosyal Bilimler Enstitüsü / Graduate School of Social Sciences	
Uygulamalı Matematik Enstitüsü / Graduate School of Applied Mathematics	
Enformatik Enstitüsü / Graduate School of Informatics	
Deniz Bilimleri Enstitüsü / Graduate School of Marine Sciences	

YAZARIN / AUTHOR

Soyadı / Surname : Türkmenoğlu
Adı / Name : Evren
Bölümü / Department : Arkeometri

TEZİN ADI / TITLE OF THE THESIS (**İngilizce** / English) : PALEOCLIMATIC INVESTIGATION OF KARAIN CAVE (ANTALYA) USING STALAGMITE DATA

TEZİN TÜRÜ / DEGREE**:** **Yüksek Lisans** / Master [x] **Doktora** / PhD [ ]

1. **Tezin tamamı dünya çapında erişime açılacaktır. /** Release the entire work immediately for access worldwide. [x]
2. **Tez iki yıl süreyle erişime kapalı olacaktır.** / Secure the entire work for patent and/or proprietary purposes for a period of **two year. *** [ ]
3. **Tez altı ay süreyle erişime kapalı olacaktır.** / Secure the entire work for period of **six months**. ***** [ ]

***** *Enstitü Yönetim Kurulu Kararının basılı kopyası tezle birlikte kütüphaneye teslim edilecektir.*
A copy of the Decision of the Institute Administrative Committee will be delivered to the library together with the printed thesis.

Yazarın imzası / Signature ..... **Tarih** / Date 26/02/2024